Planet. Space Sci., Vol. 36, No. 11, pp. 1229–1253, 1988
Printed in Great Britain.

0032-0633/88 $3.00 + 0.00
Pergamon Press plc

ION FLOWS AND HEATING AT A CONTRACTING POLAR-CAP BOUNDARY

M. LOCKWOOD*
Rutherford Appleton Laboratory, Chilton, Didcot, OX11 0QX, U.K.

S. W. H. COWLEY and H. TODD
Blackett Laboratory, Imperial College, London, SW7 2BZ, U.K.

D. M. WILLIS
Rutherford Appleton Laboratory, Chilton, Didcot, OX11 0QX, U.K.

and

C. R. CLAUER
STAR Laboratory, Department of Electrical Engineering/SEL, Stanford University, Stanford, CA 94305, U.S.A.

(*Received* 6 *July* 1988)

Abstract—Data recorded by the POLAR experiment run on the EISCAT radar during the international GISMOS campaign of 3–5 June 1987 are studied in detail. The polar-cap boundary, as defined by an almost shear East–West convection reversal, was observed to jump southward across the EISCAT field of view in two steps at 02:00 and 03:00 Magnetic Local Time and subsequently to contract back between 04:00 and 07:00 M.L.T. An annulus of enhanced ion temperature and non-thermal plasma was observed immediately equatorward of the contracting boundary due to the lag in the response of the neutral-wind pattern to the change in ion flows. The ion flow at the boundary is shown to be relatively smooth at 15 s resolution and directed northward, with velocities which exceed that of the boundary itself. The effect of velocity shears on the beamswinging technique used to derive the ion flows is analyzed in detail and it is shown that, for certain orientations of the cap boundary, spurious flows into the cap can be generated. However, these are much smaller than the observed flows into the polar cap and cannot explain the potential difference across the observed segment of the cap boundary (extending over 2 h of M.L.T.) which is roughly 7 kV. Similarly, an observed slowing of the zonal flow near the boundary cannot be explained as an error introduced by the use of the beamswinging technique. The results could be interpreted as being due to reconnection occurring on the dawn flank of the magnetopause (mapping to the polar cap at 04:30–06:30 M.L.T.). However, they are more consistent with recent observations of slow anti-sunward flow of closed field lines on the flanks of the geomagnetic tail, which appears to be generated by some form of "viscous" coupling to the magnetosheath plasma.

1. INTRODUCTION

Observations of plasma convection in the high-latitude ionosphere have revealed two types of flow reversal close to the poleward edge of the auroral oval: rotational reversals, where the velocity rotates from one zonal sense to the other through a meridional flow, and shear reversals where no rotation is observed. In studies of plasma convection, it is common to refer to these reversals as the "polar-cap boundary" and for a shear reversal this boundary is an equipotental contour. Rotational reversals are found near the dayside merging gap, or "throat", and at the nightside reconnection region (which map to the dayside magnetopause and the tail neutral line, respectively). Shear reversals are observed by satellites nearer dawn and dusk (Heelis *et al.*, 1976, 1982; Heelis and Hanson, 1980). Ground-based incoherent scatter radars, on the other hand, have tended to show rotational reversals over a much larger extent of the dayside polar cap boundary (e.g. Jorgensen *et al.*, 1984), although dayside shear reversals have also been reported (e.g. Kelley, 1985) and both types of reversal are present in the dayside convection data from the Sondre Stromfjord radar, as presented by Clauer *et al.* (1984) and Clauer and Banks (1986).

In this paper we present a detailed set of observations of an almost shear flow reversal at the polar cap boundary, observed near dawn using the EISCAT radar. This study will include: 2.5 min resolution

* Also Visiting Honorary Lecturer at Blackett Laboratory, Imperial College, London SW7 2BZ, U.K.

vector data on (1) the nature of convection at this boundary and (2) on the motion of the boundary itself; (3) 15 s resolution line-of-sight velocity data at and near the boundary; and (4) observations of the changes of ion temperature and ion velocity distribution caused by the motion of the boundary. The following subsections give an introduction to each of these areas in turn.

1.1. *Convection cells driven by "viscous interaction" at the magnetopause*

There is an important difference between the above definition of the polar-cap boundary (in terms of the pattern of high-latitude plasma convection) and the boundary between open and closed field lines. The latter will only coincide exactly with the flow reversal for purely reconnection-driven convection. Studies of the dependence of the cross-cap potential on the interplanetary magnetic field (IMF) have shown that, although convection is mainly driven by reconnection (Reiff *et al.*, 1981, 1985; Sergeev and Kuznetsov, 1981; Wygant *et al.*, 1983; Doyle and Burke, 1983; Cowley, 1984, 1986), there is residual anti-sunward convection when the IMF is northward (an orientation for which little or no reconnection is expected at the subsolar magnetopause). When allowance is made for the influence of open field lines which remain connected to the IMF after it has turned northward at the subsolar magnetopause, it is found that only roughly 15–25 kV of the transpolar potential (which, to within the magnitude of any field-aligned potential differences, equals the cross-magnetosphere potential) cannot be explained by reconnection, compared with the 60–100 kV typical of southward IMF. This residual potential has been ascribed to a "viscous-like interaction", of the kind suggested by Axford and Hines (1961), acting on the flanks of the magnetopause where reconnection is not occurring (Crooker, 1977). This has been included in a model of the convection pattern by Reiff and Burch (1985) as "viscous-interaction cells" in addition to the main dawn and dusk cells (driven by reconnection at the subsolar magnetopause) and "lobe cells" (driven by reconnection of open field lines at the sunward edges of the lobes).

Direct evidence for this viscous interaction comes from observations of anti-sunward flow on field lines which are identified as closed on the basis of the measured energy spectrum and pitch angle distribution of the energetic electron population: these have been made both at the low-latitude, near-Earth boundary layer (Eastman and Hones, 1979; Mozer, 1984, 1986; see also review by Cowley, 1986), in the far-tail boundary layer (Sanders *et al.*, 1980) and in the ionosphere (Coley *et al.*, 1987). The potential across the boundary layer was found to vary between 0 and 15 kV from *ISEE*-1 observations (Mozer, 1984, 1986), giving a peak contribution from both flanks to the total cross-cap potential of 30 kV. The average value was 3.1 kV applied across an average width at the magnetopause of 0.8 R_E. The ionospheric observations by the *DE*2 satellite reported by Coley *et al.* (1987) gave an average potential of 2.5 kV per viscous cell for the cases where such a cell could be resolved. These authors note that the narrow latitudinal width of the ionospheric projection of the viscous cell (roughly 50 km) may allow parallel potential drops to "short out" from the ionosphere some of the viscous potential and therefore they quote this value as a minimum. If fully effective, this shorting-out would cause the ionospheric signature of the viscous cell to appear as a slowing of the flow at the cap boundary, accompanied by inverted-V electron precipitation.

Details of the viscous-like interaction are not known. Penetration of solar-wind mass across the magnetopause has been suggested (Cole, 1974; Lemaire and Roth, 1978). The anomalous cross-field diffusion could be driven by electrostatic (Tsurutani and Thorne, 1982) or electromagnetic (Gendrin, 1983) waves. Other, less plausible mechanisms of mass and momentum transfer have been suggested, for example "impulsive penetration" (Heikkila, 1982; Lemaire, 1987) or "gradient-drift entry" (Olson and Pfitzer, 1985). The above theories are not really "viscous", in that mass is transferred, and all require a breakdown of the MHD "frozen-in flux" condition. The Kelvin–Helmholz instability is a mechanism which could transfer momentum without the mass transfer of the above theories (Eviatar and Wolf, 1968; Pu and Kivelson, 1983). A review of the various proposed viscous and diffusion processes, with estimates of their efficiency, has been given by Hill (1983). The patterns of convection given by the Reiff and Burch (1985) model place this viscous interaction on the dayside of the convection pattern and predict shear convection reversals at the centre of the dawn and dusk cells and shear reversals (or rotational reversals with flow out of the polar cap) on the nightside. Heikkila (1982, 1987) has suggested that the viscous interaction transfers both mass and momentum to the extent that the more distant geomagnetic tail is entirely populated with closed field lines carried anti-sunward. However, this is difficult to reconcile with a wide range of observations which are more compatible with models containing one or more reconnection neutral lines in the tail, which have been very successful in explaining a great many observed features of the tail, for example plasmoid formation and structure (see Richardson *et*

al., 1988, and references therein). However, recently, Richardson *et al.* (1988) have also reported observations of slow antisunward flows on closed field lines observed by *ISEE*-3 on the flanks of the magnetotail, both earthward and tailward of the neutral line. Antisunward flows in a far-tail boundary layer have also been reported by Sanders *et al.* (1980), the average potential of 4.2 kV in these cases being very similar to that reported closer to the Earth by Mozer (1984, 1986). In addition, Slavin *et al.* (1985) report that the average B_z component of the far-tail magnetic field near 200 R_E is negative in the centre of the tail, suggesting a location tailward of the neutral line, but positive on the flanks, indicating closed field lines. Richardson *et al.* (1988) interpret these observations as showing a viscous-like interaction across the magnetopause which transfers momentum from the solar wind into the magnetopause, but which acts on the flanks of the magnetotail, rather than at the dayside magnetopause. This transfer carries closed, previously reconnected plasma sheet flux tubes from the region earthward of the neutral line into the distant tail in a layer on one or both tail flanks. Heikkila (1986) states that most of the viscous interaction occurs in the far tail, but it seems highly unlikely that this maps to the ionospheric convection throat region, as he suggests (Mozer, 1986). Rather, we expect the ionospheric signature of such viscous interaction on the flanks of the tail to be a rotational reversal of flow across the boundary into the polar cap on the nightside. This process would carry closed flux tubes into the polar cap (as defined from the convection reversal), augmenting the viscously driven cells at the expense of the reconnection driven ones. In this paper we present observations of just such a signature in the midnight-to-dawn M.L.T. sector.

1.2. *Motions of the polar-cap boundary*

The latitude of the convection polar-cap boundary at a given M.L.T. is known to be highly variable, as is expected when dayside merging is not balanced by nightside reconnection. For example, using data from the EISCAT and Sondre Stromfjord incoherent radars and from the *Dynamics Explorer* 1 satellite, Lockwood *et al.* (1986) deduced a large-scale polar-cap expansion, consistent with the application of 150–200 kV across the polar cap. The expansion was described by the model of Siscoe and Huang (1985), which assumed that the dayside merging gap was relatively narrow and did not move. The cap boundary away from the merging gap is then described as "adiaroic" (meaning "not-flowing across"), i.e. the boundary moves with the convection speed of the plasma. In the example discussed by Lockwood *et al.* (1986) the Sondre Stromfjord radar observed the motions of the plasma and the cap boundary motion in the middle of the afternoon sector; both were found to be directed southward with similar speeds, i.e. the boundary was adiaroic. At the same time, EISCAT observed flow out of the expanding polar cap in the pre-midnight sector, showing nightside reconnection. Conversely, in another example of a cap expansion, observed using the Sondre Stromfjord radar at roughly the same M.L.T. in the afternoon sector and following a southward turning of the IMF, de la Beaujardiere *et al.* (1987) reported that the flow at the boundary was northward, while the boundary moved southward. Hence in this second example the boundary is certainly not adiaroic. These observations imply that merging was occurring on field lines which map to the middle of the afternoon sector in the ionosphere for the event discussed by de la Beaujardiere *et al.* (1987) but not for that discussed by Lockwood *et al.* (1986).

Large-scale expansions and contractions of the polar cap have also been deduced by Holzer *et al.* (1986) from the precipitation boundaries observed by two *DSMP* satellites and shown to be consistent with conservation of open flux (equivalent to Faraday's Law), using IMF and westward electrojet current observations to quantify dayside merging and tail reconnection rates, respectively. A review of the observed responses of the polar cap—expansions, contractions and distortions—to changes in the IMF has been given recently by Lockwood and Freeman (1988).

1.3. *High-time resolution observations of plasma flow in the vicinity of the polar-cap boundary*

The temporal variability of ionospheric convection, observed with 15 s resolution, has recently been surveyed by Todd *et al.* (1988) using data from the POLAR experiment run on the EISCAT radar. The POLAR field-of-view (f-o-v) was found to rotate into distinct regions of plasma flow at different U.T. Near magnetic noon, very low flow speeds were generally observed as the f-o-v is between the two cells, equatorward of the merging gap. However, bursts of poleward flow are observed in this M.L.T. sector and these are thought to be the low-latitude part of the ionospheric signature of Flux Transfer Events (FTEs) at the dayside magnetopause (Todd *et al.*, 1986), as predicted by Southwood (1985, 1987). As a result, the plasma flow at the polar-cap boundary itself is also expected to exhibit strong impulsive bursts at these times, due to isolated reconnection events (the FTE model of Russell and Elphic, 1978) or due to variations of reconnection rate over a broader longi-

tudinal extent (Southwood *et al.*, 1988). Observations of impulsive flow bursts across the polar-cap boundary on the dayside have been presented by Goertz *et al.* (1985). It is not known if the flow at the polar-cap boundary at M.L.T. outside the merging gap shows similar impulsive bursts. Lockwood *et al.* (1988a) have considered the flow which would be induced near the dawn or dusk polar-cap boundary by the passage of an FTE formed near the subsolar magnetopause and subsequently dragged dawnward or duskward round the low-latitude magnetopause, as predicted by Cowley (1986). Todd *et al.* (1988) also note a channel of strong convection at the centre of the auroral oval, where the ion flows show other large fluctuations at Pc5 frequencies. However, as the POLAR f-o-v approaches the polar-cap boundary near dawn or dusk, the flows become smoother, with little or no such fluctuations. The observations of the polar-cap boundary near dawn presented here are the first to look at the cap boundary away from the merging gap with this high-time resolution.

1.4. *Ion heating due to motions of the polar-cap boundary*

The implications of large-scale expansions and contractions of the polar cap, as discussed in Section 1.2, for ion heating and the formation of non-thermal ion velocity distributions was considered theoretically by Lockwood and Fuller-Rowell (1987a, b). Non-thermal plasma has been observed by EISCAT, when operating in the POLAR mode, during periods of strong ion heating (Lockwood *et al.*, 1987, 1988b, c). Near dawn and dusk, Lockwood and Fuller-Rowell predicted that a band of high ion temperatures, probably containing non-thermal plasma, would form on the low-latitude side of a contracting polar-cap boundary and on the high-latitude side of an expanding boundary. This behaviour is a simple consequence of the inability of the neutral-wind pattern to respond to changes in cross-cap potential as rapidly as can the plasma-convection pattern.

In this paper we present EISCAT observations of a contracting polar-cap boundary near magnetic dawn. The nature of the ion flows at this boundary are discussed, making use of inferences from the observed ion heating. Following a description of the POLAR experiment and an overview of the period of interest in Section 2, we consider the possible errors introduced by the beamswinging technique employed to derive 2.5 min resolution flow vectors in Section 3. The nature of the flow reversal at the boundary and any flows across the boundary are then discussed in Section 4 and the variability of the flow at and around the boundary is assessed in Section 5 from 15 s resolution line-of-sight velocities. In Section 6 we consider the ion heating which results from the observed contraction of the boundary.

2. OBSERVATIONS

The observations presented in this paper were made using the EISCAT Special Programme POLAR, using radar time contributed by all six EISCAT Associates. The period of observations, 3–5 June 1987, was part of an international GISMOS campaign (Global Ionospheric Simultaneous Measurements Of Substorms), during which observations were also made by a variety of other radars (including Sondre Stromfjord, Millstone Hill, STARE, SABRE and Goose Bay) and by ground-based magnetometers. The interplanetary medium was monitored by the *IMP*-8 satellite and auroral images were obtained by the *Dynamics Explorer* 1 satellite. The period of particular interest to this paper (1–5 U.T. on 5 June 1987) will also be discussed by Clauer *et al.* (1988), who will consider the global convection changes, using the EISCAT data in conjunction with all the other ground-based and satellite data accrued at this time. These combined data tell us much about the conditions which caused the polar-cap boundary to contract rapidly across the POLAR f-o-v. In this paper, we will concentrate on the nature of the boundary and the ionospheric effects seen by EISCAT in association with this contraction.

The POLAR experiment has been described by van Eyken *et al.* (1984) and Willis *et al.* (1986). It employs the monostatic beamswinging technique to evaluate ion-flow vectors and other plasma parameters to the North of Tromsö. The beamswinging cycle is 5 min long, with dwells at two azimuths, 24° apart. The azimuths employed have been chosen such that observations at a given range along both are made on the same L-shell. Each dwell lasts 2 min and is followed by a 30 s period during which the antenna is in motion. Assuming the field-aligned flow is negligible, a field-perpendicular vector is derived every 2.5 min, by combining the dwell-averaged line-of-sight (l-o-s) velocity with an interpolated value from the two adjacent dwells at the other azimuth. This also assumes that the flow is uniform across the f-o-v and constant over the beamswinging cycle period. However, it should be noted that vectors containing completely independent information are only obtained once every 7.5 min. In addition, POLAR makes l-o-s velocity measurements every 15 s and these have been used by Todd *et al.* (1986, 1988) to deduce features of the flow at much higher time resolution. When considered this way, POLAR is giving 15 s scalar information from two spatially separated locations. The observations are made using a beam elevation of 21.5° and 12 receiver

gates, each 75 km long with centres at ranges $450+75n$ km (where n is gate number), invariant latitudes $70.2+0.6n°$, and altitudes $175+35n$ km, approximately. The beam makes an angle in the range 70–74° with the geomagnetic field, depending on n and azimuth.

An overview of the POLAR data for 4–5 June 1987 is presented in Fig. 1, which shows 10 min averages of vector velocity, **v**, and 2 min averages of plasma density, N_e, electron temperature, T_e, and ion temperature, T_i. The figure uses the concentric M.L.T.-invariant latitude polar dial format described by Willis *et al.* (1986). The scalar plasma parameters, N_e, T_e and T_i, have all been determined with the assumption that the ion velocity distribution is Maxwellian (see Section 6). Between 12:00 and about 21:00 M.L.T., the data show strong sunward convection (westward, coloured green), typical of POLAR observations of the dusk cell in this sector (see statistical survey by Etemadi *et al.*, 1988b). In this period, the flows generally have little or no latitudinal variation in speed, suggesting the cap boundary remains to the North of the f-o-v. The decrease in speeds noted by Etemadi *et al.* (1988b) and Todd *et al.* (1988) as the f-o-v approaches the cap boundary is observed near 20:00 M.L.T. on this day. However, westward flow persists, with only a few minor interruptions, until strong eastward flow is established at 00:30 M.L.T. The dawn-cell auroral oval flows are interrupted at 02:00 M.L.T. when a reversal to eastward convection, thought to be the polar-cap boundary, jumps equatorward to the centre of the f-o-v, where it remains until 03:00 M.L.T. At this time the flow boundary jumps further equatorwards, giving westward polar cap flow at all latitudes within the f-o-v, whereas POLAR usually observes eastward flow at these times (e.g. Lockwood *et al.*, 1986). At 04:30 M.L.T., the reversal begins to move poleward across the f-o-v. After an initial rapid contraction of the boundary at this time, there is little motion across the f-o-v between 05:00 and 06:00 M.L.T. In fact, this latter behaviour is roughly that expected for the rotation of the EISCAT f-o-v under a cap of constant radius and with a centre displaced by a few degrees from the invariant pole toward midnight. After 06:00 M.L.T., the boundary moves rapidly poleward and is no longer within the f-o-v after 07:00 M.L.T. Subsequently, the eastward flow of the dawn auroral zone is observed to decrease and by the end of the data the f-o-v is within the slow-flow region between the two cells (Todd *et al.*, 1988; Etemadi *et al.*, 1988b).

The second band in Fig. 1 shows that the plasma density, N_e, is reduced immediately poleward of this polar-cap boundary near dawn, but that this is not true following the two equatorward jumps of the boundary near 02:00 and 03:00 M.L.T., when the plasma density remains high in the polar cap. In addition, the innermost plot shows that a band of high ion temperature moves across the f-o-v near dawn, close to this cap boundary and where the plasma is most depleted. This suggests that the low densities may be due to enhanced loss rates caused by the increase in ion flow speed, relative to the neutrals (which also elevates the ion temperature) (Schunk *et al.*, 1975), and are not due to a plasma hole within the polar cap (Brinton *et al.*, 1978). The electron temperature plot largely reflects the height profile, with the greatest values in the furthest (highest) gate shown (gate 8). However, inspection of the data from any one gate shows that values are slightly larger when the f-o-v is in the sunward-convecting auroral oval. This may be the result of electron precipitation and/or heat conduction from the ion gas.

Figure 2 presents a more detailed view of the contraction of the polar cap and of the ion temperature enhancement, this time in a rectangular invariant latitude-U.T. frame. In order to compare Figs 1 and 2, it should be noted that M.L.T. $\approx$ U.T. $+2.5$ h, for the centre of the POLAR field of view on this day. In this figure, the 2.5 min flow vectors are given in "electric field format", with westward flow plotted up the page, and northward horizontally to the right. This prevents the largely East–West flow vectors being congested and clearly shows the flow reversal at the polar-cap boundary as a rotational reversal from westward (up the page) to eastward (down the page) via northward (to the right). The boundary appears to be close to the southward edge of the f-o-v until near 02:00 U.T. (as weak flows which fluctuate between westward and eastward are seen) after which a clear reversal is seen, first in gate 1 and then in gate 2 (the first and second horizontal rows of vectors, respectively). The flows in gate 3 then also fluctuate between westward and eastward between 02:30 and 03:30 U.T., as the cap boundary appears to move back and forth across this gate. There is a rapid poleward jump of the reversal after 03:30, followed by a short-lived expansion back across gate 4. Finally the boundary is seen to move rapidly poleward, crossing the most northerly gate shown (gate 7) near 04:15 U.T.

Also shown in Fig. 2 are colour contours of ion temperatures, observed at both azimuths. These estimates assume that the ion velocity distribution remains Maxwellian, which for ion temperatures of the displayed colour contour levels ($T_i \leqslant 1600$ K) is a good approximation and errors in T_i are small for this range ($< 10\%$). However, within the (red) band are regions were T_i greatly exceeds 1600 K, in which non-

thermal plasma is identified. In these regions the errors in T_i will be considerably greater (Raman *et al.*, 1981; Suvanto *et al.*, 1988; Lockwood *et al.*, 1988b, c), and for this reason no contours of T_i greater than 1600 K are shown in Fig. 2. This effect will be discussed further in Section 6. Note that a horizontal East–West gradient in T_i across the f-o-v appears in Fig. 2 as oscillations at the 5 min beamswinging period of the experiment. Such oscillations are particularly apparent for gates 2 and 3 in the period 02:00–03:00 U.T. However, the most obvious feature of the ion temperatures is the band of large values which always sits immediately southward of the flow reversal. In fact, the reversal coincides almost exactly with the 1300 K contour for most of the period, and at all times when the cap is contracting rapidly. Section 6 discusses why just such a band of high ion temperatures is expected immediately equatorward of this contracting polar-cap boundary, due to the response time of the neutral wind. The relationship of the convection reversal to the ion temperature enhancement is emphasized by Fig. 3, which is a plot of the 1300 K contours for the data from each azimuth in the same invariant latitude—U.T. frame as Fig. 2. Also shown are points where the zonal component of the convection along an L-shell changes sign. The relationship of these points to the polar-cap convection reversal will be discussed in Section 3: however, it can be seen that they remain at all times very close (to within about 0.25 of a degree of invariant latitude) to the points at which T_i rises above 1300 K. The ion temperature subsequently remains greater than 1300 K for a period of about 40 min.

Another striking feature of Fig. 2 are the oscillations in plasma flow with period of about 40 min which are particularly evident close to the cap boundary (e.g. gates 1–4 at 1–2 U.T.). These are also observed equatorward of the boundary, where there is considerable additional variability at lower periods. There is a general anti-correlation of flow magnitudes across the flow reversal boundary. This is most marked for pairs of gates which lie on either side of and close to the boundary (e.g. gates 2 and 4 between 2:15 and 3:15 U.T. or gates 3 and 5 between 3:15 and 4:00 U.T.) but often the effects are seen over a wider range of latitudes (compare gates 1 and 5 between 3:00 and 4:00 U.T.). Comparison with Fig. 3 shows that the flows are reduced in a given gate when the boundary moves closer to it, whereas they increase as the boundary moves away from it, and motions in the boundary are in phase with the long period ($\sim$40 min) oscillations in the flow near the boundary. Hence this anti-correlation shows that the boundary is a region of relatively slow flow, compared to the regions 1°–2° of invariant latitude either side of it. The following section shows that this conclusion is not just a consequence of the beamswinging technique used to derive the flows. The westward flows in the polar cap are very uniform and constant, and tend to show only reductions from their constant value as the boundary approaches—these reductions extending over 2 or 3 gates. However the auroral, eastward flows show periods of enhanced velocity, not just reductions. A notable example of this is gates 2 and 3 during the brief northwards excursion of the boundary shortly after 03:30 U.T.: the flow speeds in gate 2 reach over 2.9 km s^{-1} at these times.

3. EFFECT OF THE BEAMSWINGING TECHNIQUE ON OBSERVED FLOWS AT A SHEAR BOUNDARY

The vector flows described in the previous section were all derived using the beamswinging technique. This assumes that the velocity is uniform over the f-o-v and that it is constant during the beamswinging cycle period. Neither of these assumptions is likely to be valid close to a moving polar-cap boundary. Etemadi *et al.* (1988a) have recently discussed the errors in the flow velocities which arise from temporal variations (on time scales short compared with the beamswinging period), without any spatial variations across the f-o-v. They concluded that although the lag giving peak correlation of the flow with some independent variable (e.g. IMF B_z) is not altered by the beamswinging technique, this is certainly not true for the direction and magnitude of the inferred flow at times close to a change in real flow. Clauer and Banks (1986) have considered the errors introduced by spatial variations in the flow within the f-o-v.

In this section we consider how the beamswinging technique, as used in the POLAR experiment and hence in the analysis employed to derive the vectors in Figs 1 and 2, can affect the deduced flows when a shear reversal boundary moves across the f-o-v. In order to do this, we simulate the effects of a 180° shear boundary moving poleward, such that its intersection with the normal to the L-shell moves with speed V_b (positive northwards) in a frame of reference fixed with respect to the radar. The boundary is also inclined at an angle α to the L-shell (see Fig. 4). Note that the definition adopted allows V_b to be measured directly from Fig. 2, whereas the speed of the boundary normal to itself, $V_b \cos\alpha$, is not measurable (as the angle α is not generally known). The flows on either side of the boundary are parallel to the boundary in the frame of reference moving with the boundary (i.e. it is a shear reversal in this frame). Equatorward and poleward of the boundary the zonal

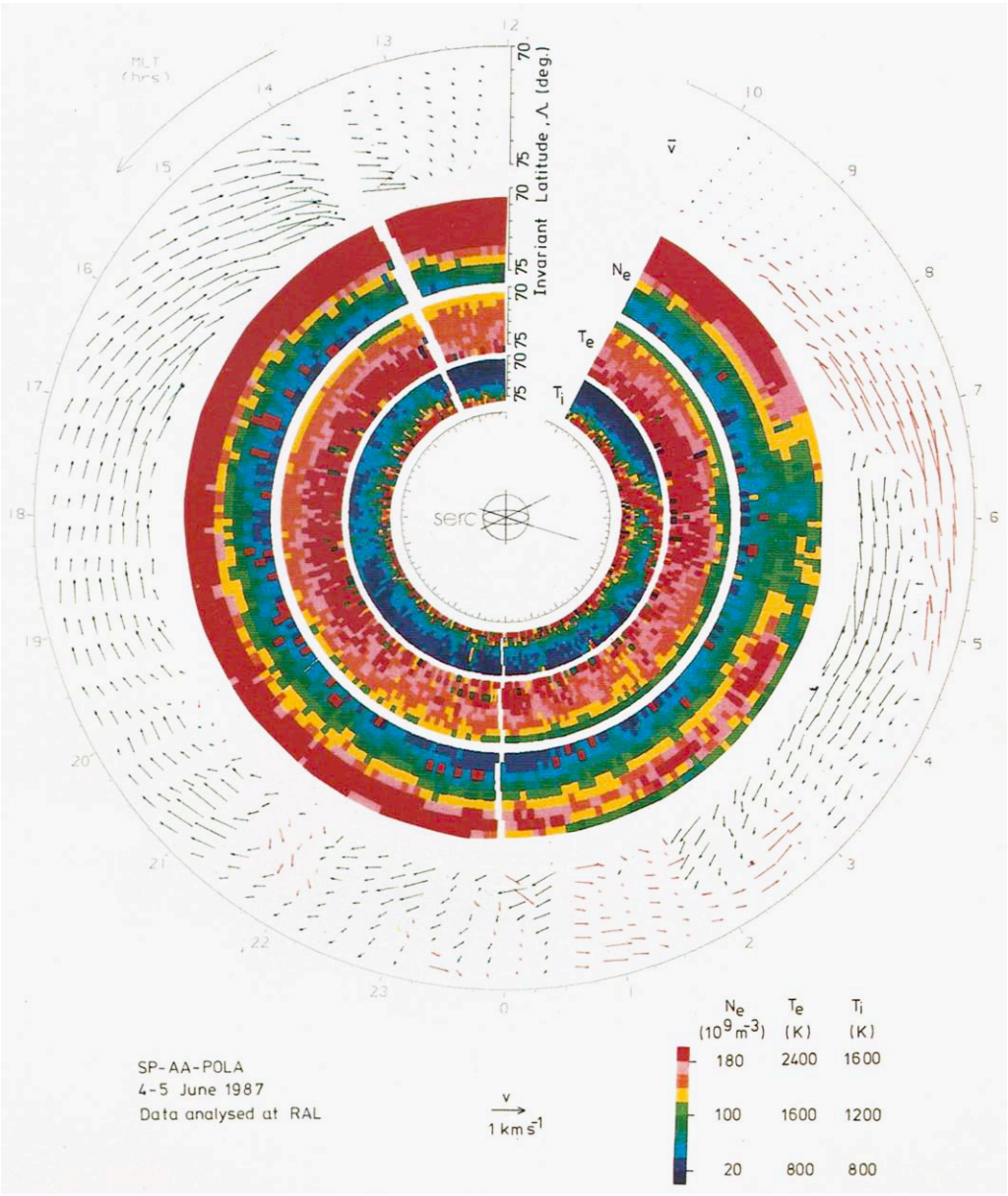

FIG. 1. POLAR DIAL PLOT OF EISCAT DATA FOR THE PERIOD 10 U.T. ON 4 JUNE 1987 TO 8 U.T. ON 5 JUNE. The data are presented as concentric M.L.T.-invariant latitude plots of the plasma velocity, V (10 min averages), plasma density, N_e, electron temperature, T_e, and ion temperature, T_i. The invariant pole is at the centre of each plot, but the invariant latitude scale is different for each, and given along the noon M.L.T. axis. The scalar data (N_e, T_e, T_i) are 2 min integrations for azimuth 332° only (data for azimuth 356° are similar). Flow vectors which are westward of the normal to the L-shells are coloured green, those eastward are red.

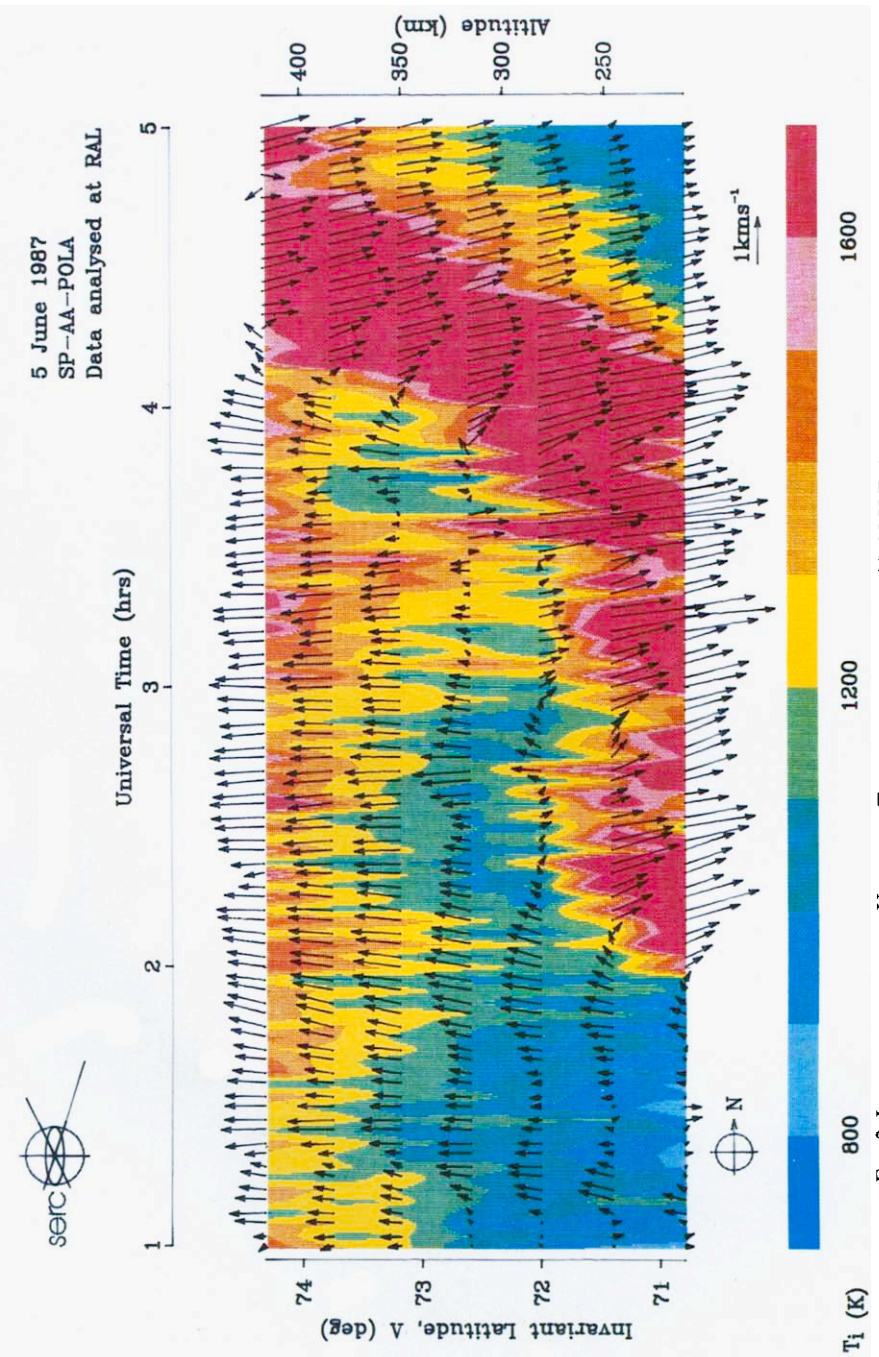

FIG. 2. INVARIANT LATITUDE—UNIVERSAL TIME PLOT OF THE PERIOD 01–05 U.T. (ROUGHLY 03:30–08:30 M.L.T.). Plasma flow vectors at 2.5 min resolution are plotted with westward flow up the page and northward flow horizontally to the right, with scale 1 km s^{-1} vector given toward the bottom right of the figure. The vectors are superposed on a colour contour map of the ion temperatures, derived for both azimuths with the assumption that the ion velocity distribution is Maxwellian. The ion temperature scale is given along the bottom of the plot. The polar-cap boundary reversal from westward to eastward flow, is seen to move northward across the f-o-v between roughly 02:00 and 04:00 U.T.

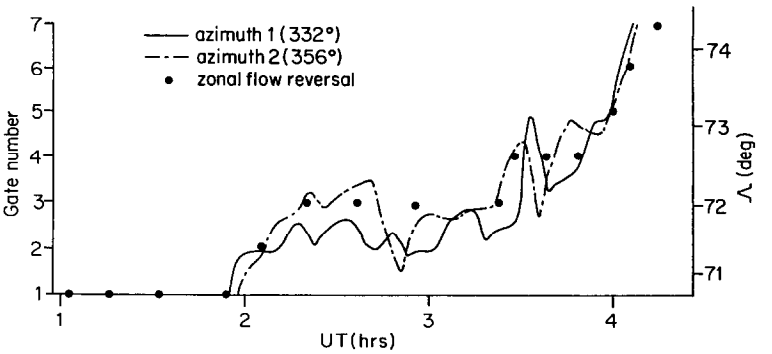

FIG. 3. THE 1300 K CONTOUR OF ION TEMPERATURE, T_i, ON THE SAME INVARIANT LATITUDE—U.T. FRAME AS FIG. 2, FOR AZIMUTH 1 (332°—SOLID LINE) AND AZIMUTH 2 (356°—BROKEN LINE).
Also shown are the points for each range gate where the zonal convection component, along the L-shell, reverses sense.

component, along the L-shell, is eastward and westward respectively: the convection speeds in the moving boundary frame are V_a' and V_c' (subscripts a and c referring to "auroral" and "cap" regions, respectively) which transform to V_a and V_c in the frame fixed with respect to the radar:

$$\mathbf{V}_a = V_a' \cdot \mathbf{t} + V_b \cos\alpha \cdot \mathbf{n},$$

$$\mathbf{V}_c = -V_c' \cdot \mathbf{t} + V_b \cos\alpha \cdot \mathbf{n}$$

where $\mathbf{t}$ is a unit vector tangential to the boundary in the eastward direction and $\mathbf{n}$ is a unit vector normal to the boundary in a northward direction.

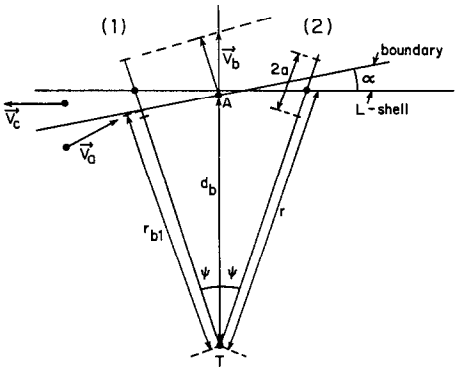

FIG. 4. GEOMETRY OF THE MODEL CAP BOUNDARY, RELATIVE TO THE POLAR BEAM DIRECTIONS, (1) AND (2), IN THE ELEVATION PLANE OF THE OBSERVATIONS.
The look directions are $\Psi = 11°$ on either side of the L-shell meridian (AT). The boundary velocity, $\mathbf{V}_b$, and the convection velocities in the auroral oval and polar cap, $\mathbf{V}_a$ and $\mathbf{V}_c$, are all in the frame which is fixed with respect to the radar at Tromsö (T). Transformed into the moving boundary frame, the convection velocities become $\mathbf{V}_a'$ and $\mathbf{V}_c'$ which are antiparallel—i.e. the boundary is a shear reversal. A range gate is $2a$ long, centred on a range r. The boundary is inclined at an angle α to the L-shell and intersects the beam directions at r_{b1} and r_{b2}, and the L-shell meridian through Tromsö at a distance d_b from Tromsö (T).

The boundary described here would be expected between the auroral oval and the polar cap near dawn for the Heelis *et al.* (1982) convection model, while the polar cap is shrinking.

Figure 4 defines the variables used and the geometry of the boundary relative to the POLAR look-directions. The angle between the boundary and the L-shell is α and the angle Ψ, between the look-directions (1) and (2) and the normal to the L-shell, is 11° in the elevation plane of the observations. The boundary is taken to be straight over the f-o-v.

For a given polar-cap boundary location and orientation across the f-o-v, it is necessary to compute the 2 min integrations of line-of-sight velocities observed along each azimuth, V_1 and V_2. These are combined to give the northward and eastward flows using the equations given by van Eyken *et al.* (1984) but with the value deduced for one dwell combined with the linearly interpolated value for the two adjacent dwells at the other azimuth, as described by Willis *et al.* (1986). This was the procedure used to derive the flow vectors shown in Fig. 2. It is not possible to simulate the l-o-s velocities in a fully rigorous and general manner, as factors like a large plasma density variation across the shear can become important. Hence a simplified approach is used here. Figure 4 demonstrates that a range gate, of total length $2a$, can straddle a shear flow reversal for one or both of the azimuths. In such cases, information is taken from both sides of the boundary, even in a single recorded auto-correlation function (acf) from that range gate. Hence the shear can affect the determined l-o-s velocity, in addition to causing errors if l-o-s velocities from both sides of the boundary are combined by the

beamswinging technique. For density observations (from the zero lag of the acf) a is 75 km for POLAR, falling to 50 km for the longest (sixteenth) lag. Analysis of POLAR data using various numbers of lags shows the optimum number for velocity determination is about twelve, but that most of the velocity information is contained in the first three or four lags (B. J. I. Bromage, private communication). Here we adopt a weighting for l-o-s velocity measurements which is the same as that appropriate to the zero lag (density measurement). This gives a maximum spread of locations over which a shear can affect a range gate ($a = 75$ km) and full lag analysis justifies this approach as the l-o-s velocity weighting is found to be very similar to the triangular weighting for the density (P. J. S. Williams, private communication). It is straightforward to allow for range-squared (spatial signal attenuation) corrections of the weighting across the gate, which are relatively long for POLAR compared to other EISCAT experiments. Further refinement of the computation of weighting functions is not considered worthwhile, bearing in mind that a range gate covers a range of altitudes and invariant latitudes and hence spatial variations in plasma density will, in practice, also influence the relative weight given to each part of a gate divided in two by the flow boundary. By integrating over the range gate, this simplified approach gives a weighting factor to that part of the gate in the auroral oval of:

$$w_a = \frac{1}{c}\left[\frac{r-a}{r_b} + \log_e \frac{r_b}{r-a} - 1\right] \quad r_b < r$$

$$w_a = \frac{1}{c}\left[\frac{a(a+r_b-r)}{r_b(r-a)} + \log_e\left[\frac{r^2}{r_b(r-a)}\right] - \frac{r(r+r_b-a)}{r_b(r-a)} + 2\right] \quad r_b > r \quad (1)$$

where

$$c = \log_e\left[\frac{r^2}{r^2-a^2}\right],$$

r is the range of the centre of the gate, and r_b is the range of the boundary along the look direction (defined for azimuth 1, r_{b1}, in Fig. 4). The weighting function is averaged to allow for the variation of the distance r_b (due to the motion of the boundary) during each 15 s pre-integration period. The weighting factor for that part of the gate in the polar cap is $w_c = 1 - w_a$.

The l-o-s velocities, V_1 and V_2, are determined from 2 min post-integrated acfs by a matched-filter technique: as a result, this post-integration can be simulated by averaging the 15 s values. Instantaneous values of the l-o-s velocities are obtained from V_a and V_c by averaging using weighting functions w_a and w_c. The V_1 and V_2 values are then combined to give the flow vector in the same way as the experimental values, as described above.

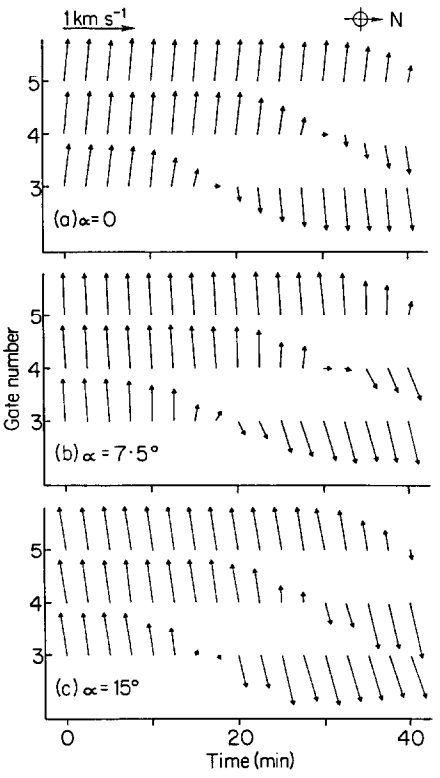

FIG. 5. SIMULATED FLOW VECTORS.
These are shown for range gates 3, 4 and 5 (r = 675, 750 and 825 km) in the same format as for Fig. 2, for model values $\mathbf{V}_b = 100$ m s^{-1}, $V_c' = V_a' = 1$ km s^{-1} and α of (a) 0°, (b) 7.5° and (c) 15°.

Some simulated vectors are shown in Fig. 5 as a function of time for flow speeds (in the reference frame for which the boundary is at rest) within the polar cap and auroral oval, $V_c' = V_a' = 1$ km s^{-1} and northward boundary speed $V_b = 100$ m s^{-1}. The vectors are shown for three range gates (3, 4 and 5, for which r = 675, 750 and 825 km) for three boundary orientations, with α positive (negative values are not expected at the M.L.T. of the observations, however, their possible effects will be discussed later). The vectors are shown in the same format as Fig. 2, with northward to the right of the figure, and in the frame of reference of the radar. In all three cases the vectors rotate from westward to eastward, through northward—as for the reversals shown in Fig. 2. In part (a) of Fig. 5, the angle α is zero (boundary parallel to

the L-shell). All vectors show the correct northward component of $V_b = 100$ m s^{-1}. The only effect of the beamswinging technique is to alter the step function change in real zonal flow to a smooth variation, producing an apparent but spurious slowing of the flow at the boundary. Because the boundary is moving northward at 100 m s^{-1}, a given range gate is affected for about 12 min, corresponding to nine vectors. Note, however, that at a time when gate number n shows a zonal flow reversal, there is no effect on gates $(n-1)$ and $(n+1)$, on either side of it and that a maximum of two gates (which straddle the boundary) can be affected at any one time. As a result, we conclude that the slowing near the boundary observed in Fig. 2 is not merely a consequence of the beamswinging technique as it often extends over four or five range gates.

For parts (b) and (c) of Fig. 5, α is 7.5° and 15°, respectively. This orientation reproduces the vectors seen away from the flow reversals in the polar cap and auroral oval in Fig. 2, with nearly pure westward flow in the cap, but with flow North of eastward in the auroral oval. For both parts (b) and (c), the same basic behaviour is seen, but there is a very slight 2.5 min oscillation, which increases with increasing α, introduced into the vectors by the velocity combination algorithm.

It is found that the zonal flows do not, in general, reverse from westward to eastward at the location of the true cap boundary, although this is very nearly true for $\alpha = 0$. The separation of this derived zonal flow reversal (shown in Fig. 5) and the point A for a given gate number (the mid-point between centres of the scattering volumes for the two azimuths—see Fig. 4), Δ, is plotted in Fig. 6(a) as a function of the angle, α. It can be seen that the two agree to within 2 km for the range $-5° < \alpha < 5°$, but at very large angles of either sense, the East–West zonal flow reversal can lie 60 km equatorward of the true location of the boundary at the centre of the field of view, i.e. the true cap boundary can be roughly one range gate to the North of the derived zonal flow reversal. Part (b) of Fig. 6 shows V_s, the component of the derived flow vectors normal to the boundary minus the true plasma velocity in the same direction (the latter being $V_b \cos\alpha$). Hence V_s is a spurious flow into the polar cap introduced by the beamswinging technique. It can be seen that for $-\Psi < \alpha < \Psi$ ($\Psi = 11°$ for POLAR) V_s has magnitude less than 50 m s^{-1} and is into the polar cap for positive α (positive V_s) and out of it for negative α. Larger spurious flows into the cap can only be generated if $\alpha < -15°$, for the case with $V_c' = V_a' = 1$ km s^{-1}. Increasing V_c' and V_a' is found to cause proportional rises in V_s. This effect, along with field-aligned flows, may provide an explanation of the relative absence of shear reversals from many radar data at certain times when we would expect them from satellite data (Jorgenson *et al.*, 1984). In the following section, we study the flows across the convection reversal boundary, with careful consideration given to the effects discussed in this section.

4. DEDUCED FLOWS ACROSS THE POLAR-CAP BOUNDARY

An analysis of the plasma flow near the boundary and of the motion of the boundary is presented in Fig. 7. In part (a) it is assumed that the angle α is always zero, in which case the distance Δ is zero and average velocities of the boundary can be calculated from the intervals between zonal flow reversals in adjacent gates. The solid line in Fig. 7(a) shows this average speed of boundary motion between range gates (derived from Fig. 2), V_b, whereas the thin line shows the cross-boundary convection component (northward in this case with $\alpha = 0$), V_{cb}. This value is evaluated every 2.5 min by linearly interpolating between the two range gates adjacent to the inferred boundary location. It can be seen that the northward-directed cross-boundary convection generally exceeds the boundary speed. That this conclusion is independent of the assumed value for α is demonstrated by Fig. 7(b), which shows the potential along the cap boundary, Φ, computed in the frame moving with the boundary. Using velocities defined in the frame of the radar, this potential (across a segment of cap boundary of length L) is given by:

$$\Phi_L = \int_L (V_{cb} - V_b \cos\alpha) B \, dl \qquad (2)$$

where dl is an increment of length along the boundary and B is the geomagnetic field. In Fig. 7(b), three models of the polar-cap boundary orientation are employed which all assume that the polar cap is circular in an M.L.T.-invariant latitude frame. In the first case, the invariant co-latitude of the centre of the polar cap, θ, is taken to be zero (i.e. the cap is centred on the invariant pole), which results in α being zero at all times, as assumed in Fig. 7(a). In the other two cases θ is taken to be 3° and 6°, with the cap centre shifted towards the nightside and always on the 24 h M.L.T. meridian, giving ranges of α of 8.5°–10.6° and 18.2°–19.5°, respectively over the range of M.L.T. in which the polar-cap boundary is observed in Fig. 2. The range of θ employed here covers the majority of values derived from global auroral images by Meng *et al.* (1977). Figure 7(b) shows that the apparent potential drop across this segment of the polar cap

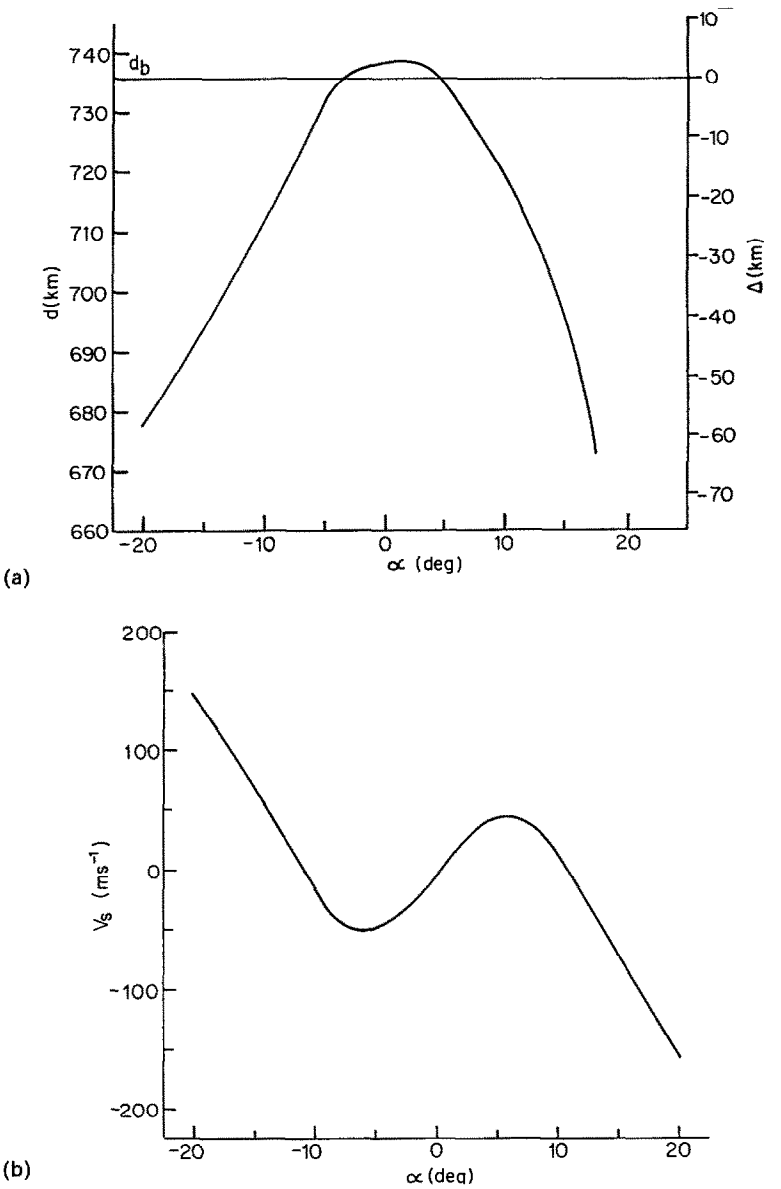

FIG. 6. (a) THE SPATIAL SEPARATION, Δ, OF THE EAST–WEST REVERSAL IN DERIVED FLOW VECTORS (AT A DISTANCE d FROM TROMSÖ) FROM THE POINT A (WHICH IS AT A DISTANCE d_b FROM TROMSÖ)—SEE FIG. 4. (b) THE SPURIOUS CROSS-BOUNDARY FLOW INTO THE POLAR CAP, V_s, AS A FUNCTION OF THE BOUNDARY ORIENTATION ANGLE, α, FOR THE RANGE $r = 750$ km AND THE SAME MODEL VELOCITIES AS FIG. 5.

does not vary greatly with the assumed model for α and is roughly 7 kV.

In Section 3, it was shown that a spurious flow into the polar cap (of speed V_s) could be generated by the beamswinging technique. The model boundary orientations used in Fig. 7(b) give spurious potential drops of 0, 1.1 and −9 kV [positive values reflecting apparent flow into the polar cap, as in Fig. 7(b)], for $V_c = 1$ km s^{-1} and $V_a = 1.5$ km s^{-1}, which apply on average to the data away from the boundary in Fig. 2. The slowing of the flows at the boundary, as inferred in Section 2, would decrease the magnitude of these spurious potentials. The worst case, which generates maximum northward flow into the polar cap, is with

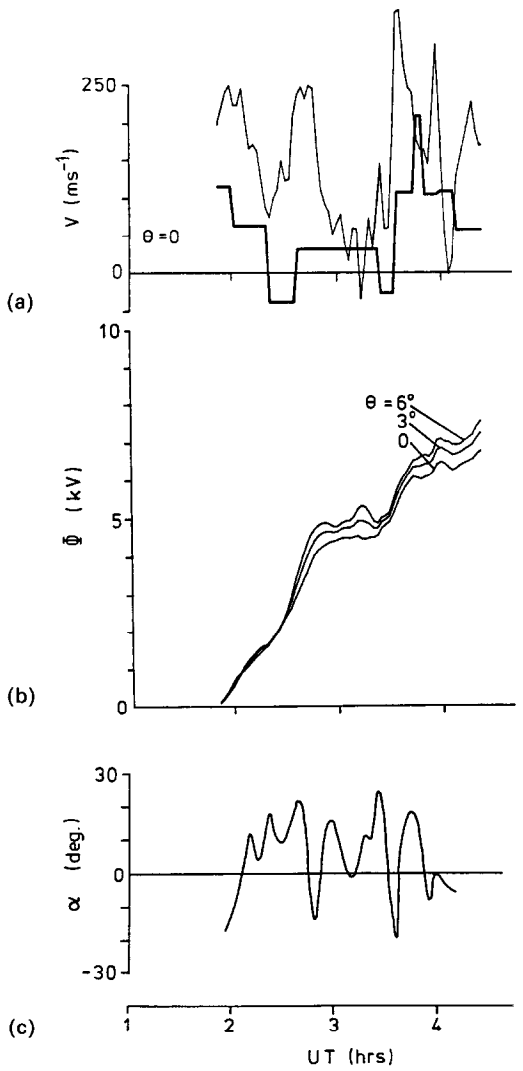

FIG. 7. ANALYSIS OF BOUNDARY MOTION AND CONVECTION NEAR THE BOUNDARY AS A FUNCTION OF U.T.
(a) Velocity components, normal to the boundary, of convection (V_{cb}; thin line) and of boundary motion ($V_b \cos\alpha$; bold line) for a circular polar cap centred at 24 h M.L.T. and invariant colatitude $\theta = 0$ (i.e. boundary orientation angle, α, always equals zero). (b) Potential along polar-cap boundary (in frame moving with the boundary), derived from integral of $(V_{cb} - V_b \cos\alpha)$, for θ of 0°, 3° and 6°. (c) Boundary orientation angle, α, inferred from ion temperature variations at the two azimuths.

$\alpha = 5.5°$ at all times (it is not considered possible for α to be less than $-15°$ for more than short periods), in which case an apparent, spurious, potential of only 3 kV is generated. Hence we conclude that the flow into the polar cap is not produced solely by the beamswinging technique.

Some information on the boundary orientation is inherent in Figs 2 and 3, which show that the ion temperature at the two azimuths is not exactly the same. Figure 2 shows that the ion temperature rise is largely coincident with the zonal flow reversal, which for small α is close to the true convection boundary [Δ is small, see Fig. 6(a)]. This is expected for a contracting cap boundary, as will be discussed in Section 6. Hence we can use the temperature rises seen at the two azimuths to determine r_{b1} and r_{b2} (see Fig. 4) at any time, and hence we can estimate α. The result is shown in Fig. 7(c). It can be seen that α fluctuates over a large range, but the average is near 12°. Because this is greater than the half-angle of beamswinging, $\Psi = 11°$, this results in a spurious potential of -0.5 kV. From the variance of the α values we deduce this spurious potential estimate has an error of roughly 1 kV, which is comparable to the uncertainty introduced into the measured Φ values by α.

Consequently, we conclude that errors introduced by the beamswinging technique cannot explain the observed flow into the polar cap and the 7 kV of potential observed along this segment of the cap boundary, although fluctuations in α, particularly the two large negative excursions inferred for two brief periods of cap expansion during the overall contraction, may well influence the temporal variation of $(V_{cb} - V_b \cos\alpha)$ shown in Fig. 7(a). These temporal variations are smoothed out by taking the integral when evaluating the potential, Φ.

5. FLOWS NEAR THE CAP BOUNDARY AT 15 s RESOLUTION

In addition to the 2.5 min resolution vector data from POLAR, there is much information to be obtained on the nature of the flows from the observed 15 s line-of-sight (l-o-s) velocities. For example, Todd *et al.* (1986) used these l-o-s velocities to detect rapid bursts of poleward flow in the auroral ionosphere, and to show that they were consistent with the expected ionospheric signature of FTEs at the dayside magnetopause. A survey of 15 s data from POLAR has been made by Todd *et al.* (1988) and has shown that flows have very different small-scale temporal and spatial structure in different parts of the convection pattern. This survey did not include observations of the cap boundary at the M.L.T. discussed here. In Fig. 8 we adopt the format of data presentation used and explained by Todd *et al.* (1988). The plots show the l-o-s velocities in the first 5 range gates for the period of Fig. 2 (1–5 U.T.). The data shown as squares are from azimuth 1 (11° to the West of the *L*-shell meridian in the elevation plane of the observations)

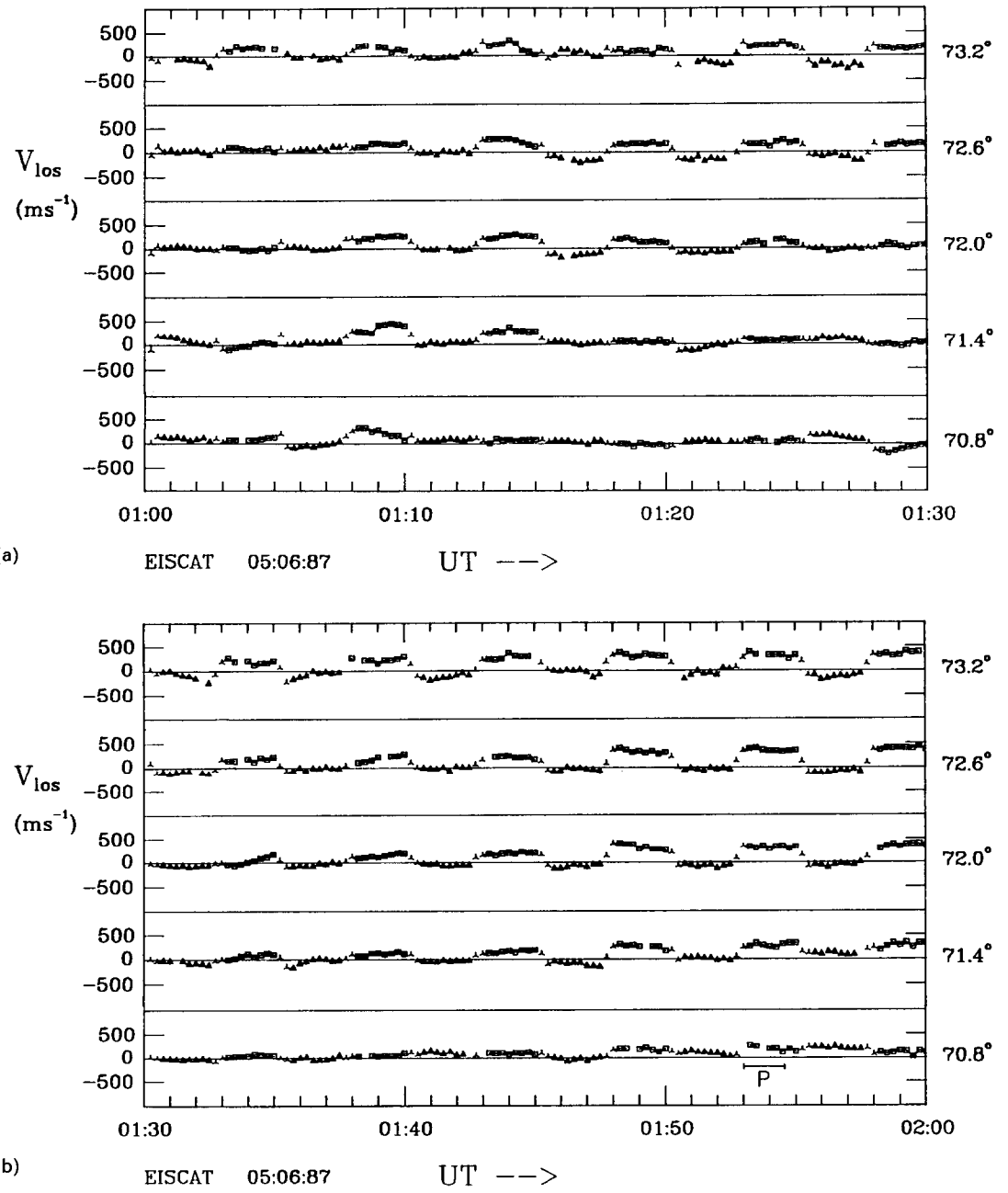

FIG. 8. 15 s RESOLUTION LINE-OF-SIGHT VELOCITIES OBSERVED DURING THE PERIOD COVERED BY FIG. 2. Squares show data from azimuth 1, triangles are from azimuth 2 (see Fig. 4).Data are shown for range gates 1 (bottom panel, $\Lambda = 70.8°$) to gate 5 (top panel, $\Lambda = 73.2°$), for the periods: (a) 1:00–1:30 U.T.; (b) 1:30–2:00 U.T.; (c) 2:00–2:30 U.T.; (d) 2:30–3:00 U.T.; (e) 3:00–3:30 U.T.; (f) 3:30–4:00 U.T.; (g) 4:00–4:30 U.T. and (h) 4:30–5:00 U.T.

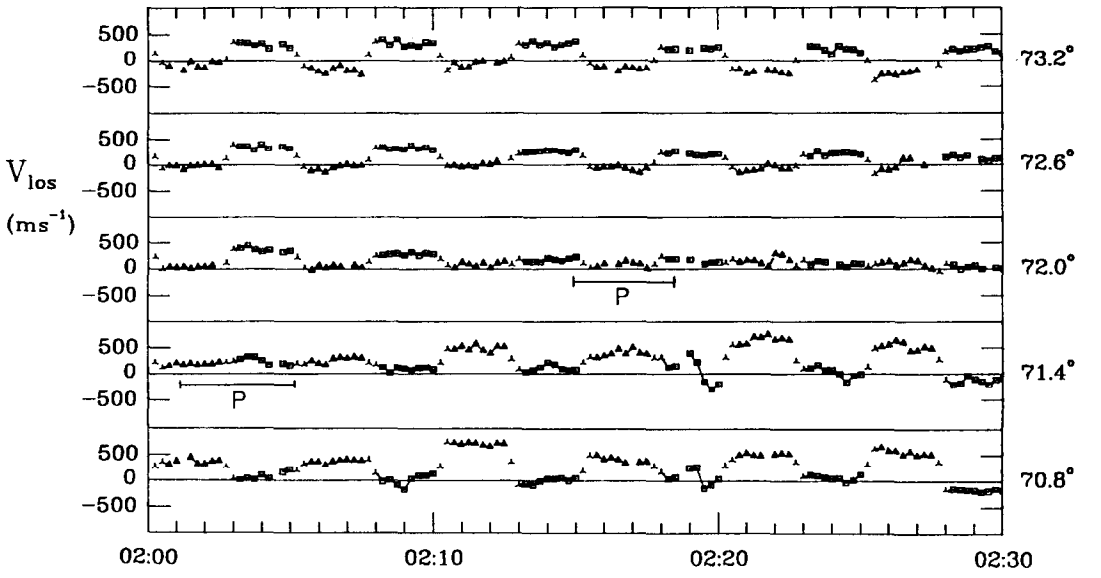

FIG. 8 (*continued*).

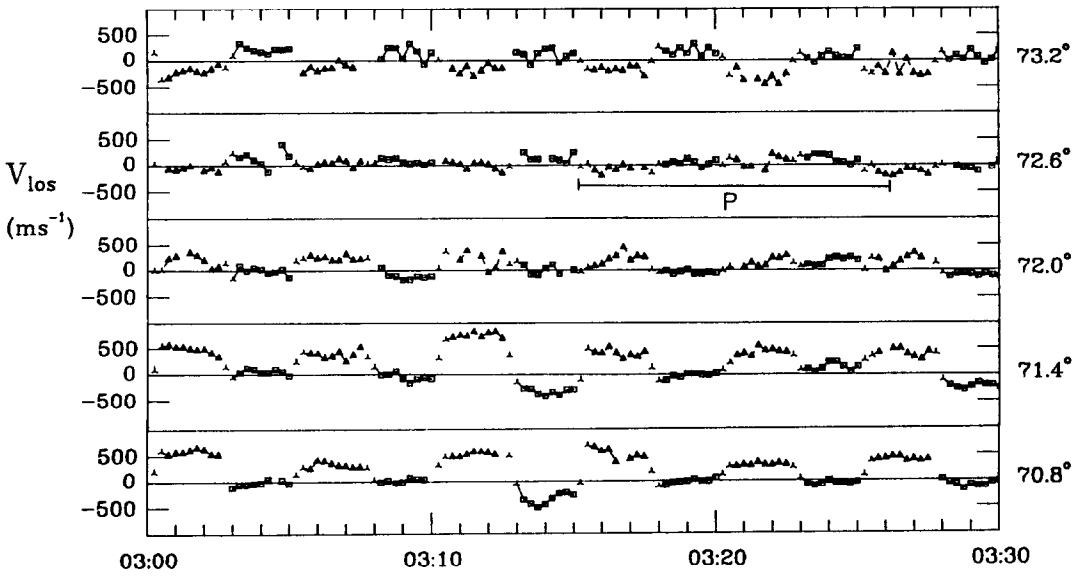

FIG. 8 (*continued*).

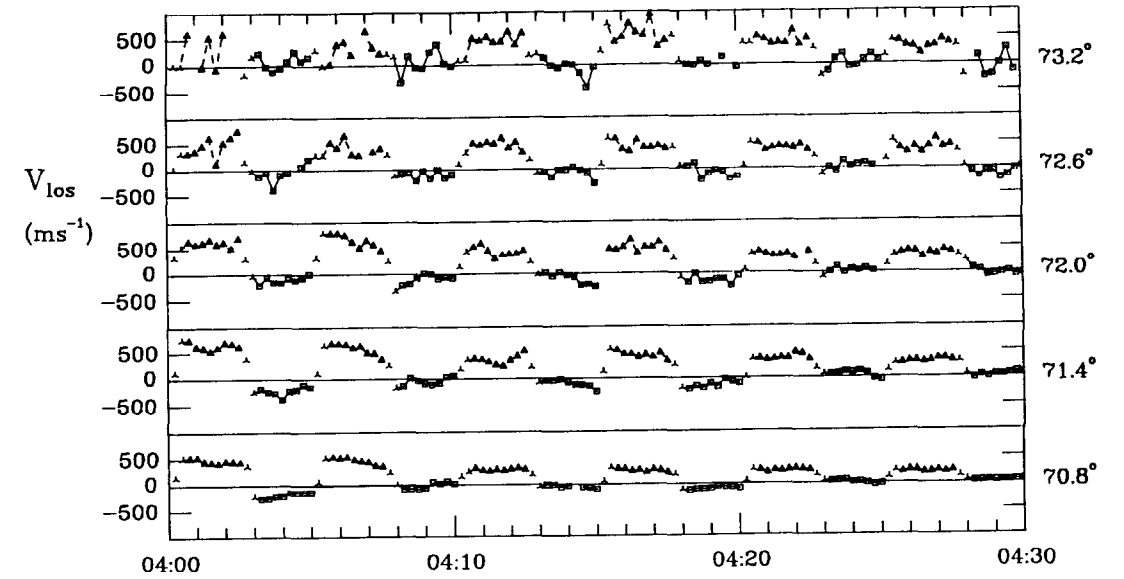

FIG. 8 (*continued*).

and those shown as triangles are from azimuth 2 (11° to the East of the L-shell meridian). The data shown as inverted-Y symbols are taken while the antenna is in motion between the two azimuths. The average point directions for these points are given in Fig. 1 of Todd *et al.* (1988).

Parts (a) and (b) of Fig. 8 cover the period 1:00–2:00 U.T., when the f-o-v is entirely within the polar cap (see Fig. 2). The data, for gates 3 and 4 in particular, show almost square-wave modulation of the l-o-s velocities introduced by the beamswinging, showing that the flow is relatively smooth (compared with the variable auroral zone flow observed at similar M.L.T. by Todd *et al.* (1988) and to that observed to the South of the cap boundary at later times in Fig. 8). Gates 1, 2 and 3 show considerable variation in the amplitude of the square wave at certain times (also seen in the vector data in Fig. 2), which we interpret as the slowing of the flows at the boundary. The lower signal-to-noise ratios of the data for gate 5 introduce more point-to-point random variability in the flows, as discussed by Todd *et al.* (1988). Overall these flows within the polar cap are very smooth and show little wave-like variation, on time-scales in the range 15 s–2 min (Fig. 2 shows there are oscillations of period 40 min).

Also marked in Fig. 8 are the times of poleward (P) and equatorward (E) motions of the convection reversal across each gate, as identified from Fig. 2. As an example of how the intervals during which these traversals occur are determined, let us look at the first, clear identification of the polar-cap boundary in Fig. 2, namely the zonal flow reversal seen at 01:54:30 U.T. in gate 1. Figure 6(a) shows that, in general the cap boundary is shifted from the location of the zonal flow reversal by a distance Δ. Because we do not know the angle α with any certainty, we do not in general know Δ. Figure 6(a) shows that the magnitude Δ is small (<30 km) for α in the range $-15° < \alpha < 15°$ and that the only large non-zero Δ values are negative. For a contracting polar-cap boundary this means that the zonal flow reversal, which lies at or equatorward of the true cap boundary, will be observed at the same time or after the true boundary is at the centre of the range gate in question. Hence Fig. 2 can only give an indication of where the cap boundary is, but not an accurate timing of its traversal of a given range gate. From the V_l values presented in Fig. 7, we can estimate the period during which the polar-cap boundary must have passed through the centre of each range gate, by assuming Δ lies in the range $-25 \text{ km} < \Delta < 0$. This calls for the traversal of gate 1 to be in the period 01:53:00–01:54:30 U.T. and inspection of Fig. 8(b) demonstrates that all data points in this period show slow, northward flow with very little point-to-point variation. The traversal periods for the other range gates were calculated in the same way and are shown in Fig. 8 by the horizontal bars. The letters P and E refer to poleward and equatorward traversals, respectively. The α angle estimates shown in Fig. 7(c) sometimes exceed 15° in magnitude, and the uncertainty in Δ could be considerably larger in such cases. Hence, the boundary may have passed a short time prior to the period shown for poleward (P) motion cases and after it for equatorward (E) motion cases. The periods marked vary in length because of the variety of deduced boundary speeds. The boundary crossings all show similar l-o-s velocity behaviour to that noted for gate 1, i.e. relatively smooth northward flow, with little point-to-point variation. This is certainly true to within experimental error of all poleward (P) traversals, but may not be true of the equatorward (E) ones. Figure 8(d) shows an equatorward crossing of gate 3 between 02:36 and 02:44 U.T., during which a burst of enhanced northward flow (up to 500 m s^{-1}) is seen around 02:37 in gates 2 and 3 (i.e. just equatorward of the boundary) with a second burst of southward flow of similar magnitude around 02:42 U.T. This variability is superimposed on a general background northward flow. Figure 7(c) shows a large and rapid oscillation in the apparent α in this period from $+20°$ to $-15°$ during this period. The only similar excursion to large negative α ($< -20°$) is also during a period of equatorward boundary motion, 03:41:30–03:50:00 U.T. [see gate 4, Fig. 8(f)]. In this latter period a similar feature is seen, but it is known the boundary must move equatorward and then return poleward again within the one period of time.

Figure 8(d) shows that considerable wave-like variations of the l-o-s velocities, with periods close to the beamswinging cycle time (5 min), occur in the first half of the period 02:30–03:00, but only in the range gates equatorward of the cap boundary (gates 1 and 2). Poleward of the boundary (gates 4 and 5) the flow shows much less sign of these oscillations (see also parts (c) and (e) of Fig. 8). Such Pc5-frequency oscillations have been reported in the centre of the auroral flow channel by Todd *et al.* (1988) at these, and other, M.L.T. It is interesting to note that there appears to be little transmission of the oscillations across the boundary: some such transmission may have been expected at least to some extent, due to the incompressible nature of the ionospheric flow, unless the oscillations were polarized in the East–West direction. It is also interesting that the amplitude of these oscillations decreases dramatically near 02:43 U.T., which is near the time that the boundary must have ceased moving equatorward, and that the inferred α value

returned from its negative excursion. Inspection of Fig. 8(f) shows that the other period of equatorward motion and negative α values also shows enhanced amplitudes at Pc5 frequencies which diminish at a time near the resumption of poleward motion. There is a clear correlation between these oscillations and the magnitude of the East–West flow (given by the separation between the l-o-s velocities for the two azimuths), as noted by Todd *et al.* (1988) and there are also certainly some oscillations at times when the boundary is moving poleward. Hence these data give an indication that boundary expansions and/or negative α (which, remember, is not the expected boundary orientation at this M.L.T.) may be associated with auroral zone flow oscillations, but a full correlative study of the Fourier components is required to establish this with certainty. Alternatively, the expansions may just bring the region of the oscillations into the f-o-v.

Part (g) of Fig. 8 shows that flow oscillations continue while the cap boundary is moving poleward, but mainly exist in the centre of the auroral flow channel, as reported by Todd *et al.* (1988). These oscillations decrease, as do the East–West flow magnitudes as the f-o-v exits the whole convection cell in Fig. 8(h).

6. ION HEATING DUE TO THE CONTRACTION OF THE POLAR CAP

Lockwood and Fuller-Rowell (1987a, b) have predicted the ion heating which would be expected in the *F*-region due to ion–neutral friction during motion of the polar-cap boundary. During a period of polar-cap contraction, there will be segments of an annulus, near dawn and dusk, where the ion flow has reversed from anti-sunward to sunward. This region lies between the original and present locations of the cap boundary. The thermospheric winds can only respond to a change in ion motions on a time scale of 10 min or greater (the time constant depending chiefly on the plasma density). Prior to the contraction, the winds in the annulus will have been generally anti-sunward, driven by both momentum transfer from the anti-sunward plasma convection and the pressure difference between the dayside and nightside due to solar heating. Hence in the poleward part of the annulus (immediately equatorward of the boundary), the ion temperature will be elevated because ion and neutral flows are in almost opposite directions, whereas immediately poleward of the boundary at any time they are in the same general direction and the ion temperature will be considerably lower. The ion temperature is elevated above the thermospheric temperature by the heating term which is proportional to $(\mathbf{V}_i - \mathbf{V}_n)^2$: Lockwood and Fuller-Rowell predict a thermospheric wind of about 400 m s^{-1} for this sector, hence for $V_a = V_c = 1$ km s^{-1}, this heating term is higher on the equatorward side of the boundary by a factor of $(1.4/0.6)^2 \approx 5.4$. Depending on the plasma density and on the rate of contraction of the boundary, the winds in the lower-latitude part of the annulus may have begun to respond to the change in ion velocity. In addition, the ion flows will be lower at large distances from the cap boundary. Consequently, it is expected that the ion temperature will be enhanced in a band of latitudes immediately equatorward of a contraction polar-cap boundary, with somewhat lower temperatures at lower latitudes in the band. Note that, conversely, a similar band of high ion temperatures would be expected immediately poleward of an expanding cap boundary.

The ion temperatures shown in Fig. 2 display exactly the behaviour predicted above, with an annulus of elevated ion temperature equatorward of the cap boundary, especially during the two periods of rapid cap contraction observed between 2:00–2:25 U.T. and 3:25–4:10 U.T. The exact coincidence of the rise in ion temperature with the zonal flow reversals indicates that the distance Δ must be small, and justifies the use of -25 km $< \Delta < 0$ in the previous section and the use of ion temperatures to evaluate α in Section 4.

Lastly, we note that the ion–neutral velocity difference is not sufficiently great to drive the plasma into a highly non-thermal state for much of the high ion temperature band ($T_i > 1600$ K). This assessment is made from visual inspection of the spectra, which take on a characteristic shape for non-thermal plasma, as predicted by Raman *et al.* (1981) and observed using the POLAR experiment by Lockwood *et al.* (1987, 1988b, c). Attempts to fit most of the spectra in the band of high ion temperatures, yield estimates of the distribution shape distortion factor, D^* (see Raman *et al.*, 1981), of typically 0.3 ± 0.3, i.e. the distribution of l-o-s ion velocities can hardly be distinguished from a Maxwellian. These fits were carried out using the procedures described by Suvanto (1988) and Suvanto *et al.* (1988). Hence the ion temperature contour levels shown in Fig. 2, which are derived assuming a Maxwellian ion velocity distribution, are not seriously in error. However, there are several "hot spots" within the band coloured red where this Maxwellian ion temperature estimate exceeds 2000 K. Inspection of the spectra at such times shows the plasma to be highly non-thermal, with fits yielding D^* values in the range 1.0–1.3. These ion temperatures are subject to up to 30% error due to the assumption of a Maxwellian distribution. The high D^* values are

found in the centre of the $T_i > 1600$ K band where the ion flows are largest, and not at its poleward edge, as would be expected from the above discussion. Hence the ion temperature and D^* values also show evidence for the slowing of the plasma flow at the boundary, in accordance with the beam-swinging flow data. Initial inspection of the ion temperature decrease on the equatorward half of the annulus shows that the response time of the neutral wind is of order 45 min in this example.

A fuller analysis of the non-thermal ion velocity distributions and ion heating during this period will be presented elsewhere. Here we just note the existence of high ion temperatures and non-thermal plasma in a band outside the contracting polar cap.

7. DISCUSSION AND CONCLUSIONS

The beamswinging technique can be used to study a shear-like polar-cap boundary, provided care is taken to ensure that possible spurious effects are not interpreted as real. It has been shown that the results summarized below cannot be explained in terms of the effects of beamswinging and a simple convection shear in the f-o-v.

The EISCAT data from the POLAR experiment described in this paper give information on the flows and ion-velocity distribution (and hence ion temperature) and show that there is a slowing of the flow near the dawn polar-cap boundary, as previously reported in the dusk auroral oval by Willis *et al.* (1986), Etemadi *et al.* (1988b) and Todd *et al.* (1988). This slowing is seen both inside and outside the cap boundary, as defined by the convection reversal, and extends over several range gates (i.e. over 1°–2° of invariant latitude), but not as many as in the previous (dusk cell) observations. Furthermore, detailed analysis of the flows at the boundary indicate a persistent poleward flow across the boundary, into the polar cap, amounting to a total potential drop of some 7 kV across the 2 h segment of the boundary observed.

There are two possible mechanisms at the magnetopause which could be invoked to explain the flow across the cap boundary. The first is reconnection, in which case the open-closed field line boundary remains co-located with the convection reversal. It is not possible from these data to establish definitively whether or not weak quasi-steady reconnection is occurring or where the open-closed field line boundary is. However, the M.L.T. of the observations would require such reconnection on the flanks of the magnetotail, in addition to that expected at the dayside sub-solar magnetopause. The width of the merging gap on the dayside is known to be very variable, for example Lockwood *et al.* (1986) and de la Beaujardiere *et al.* (1987) have presented examples of cap expansions seen at Sondre Stromfjord in the mid-afternoon sector where merging was not and was occurring, respectively, at that M.L.T. However, we are not aware of any previous observations suggesting reconnection at the M.L.T. of these observations. Data from ion drift meters on satellites have not shown flow into the polar cap at these M.L.T. (e.g. Heelis and Hanson, 1980), which would suggest that this is not a common occurrence. Furthermore, reconnection would give a sharp boundary between sunward convecting closed field lines and open field lines which would be dragged anti-sunward as soon as they were merged with the IMF. There are therefore difficulties in explaining the observed slowing of the flow at the boundary in terms of reconnection.

The second mechanism which can be invoked to explain the flow into the polar cap is a viscous-like interaction at the magnetopause. Three separate hypotheses have been made for the necessary momentum transfer at the magnetopause: penetration of solar wind plasma filaments into the magnetosphere, wave-driven diffusion and boundary waves (in particular Kelvin–Helmholtz waves, see introduction Section 1.1). Recent analysis of *ISEE*-3 data from the distant ($\sim 200\ R_E$) tail, carried out as part of the CDAW-8 workshop, has provided evidence for viscous-like interaction on the flanks of the magnetotail (Richardson *et al.*, 1988). This evidence takes the form of observations of a thick (of order 10 R_E) layer of closed plasma sheet flux tubes flowing slowly anti-sunward on the flanks of the tail. The antisunward flow speed of this plasma (100–200 km s^{-1}) is much less than that occurring tailward of the neutral line (400–600 km s^{-1}) in the central region of the tail at these distances, such that Richardson *et al.* (1988) termed these flows the "slow plasma sheet". The observations indicate that this population originates from the closed plasma sheet flux tubes located earthward of the neutral line, which initially flow earthward after reconnection, but are subsequently carried tailward, presumably by "viscous" coupling to the solar wind flow across the flanks of the tail, as is shown schematically in Fig. 9(a). This interpretation differs from that of Heikkila (1982, 1986), who proposed that the flank layers are formed by the tailward transport of closed, dayside flux tubes, a proposal which is not supported by the *ISEE*-3 tail data. A schematic of this flow pattern is given in part (a) of Fig. 9, which shows a snapshot of the inferred flow streamlines in the equatorial plane. The flanks of the magnetopause are depicted with wavy lines because Richardson *et al.*

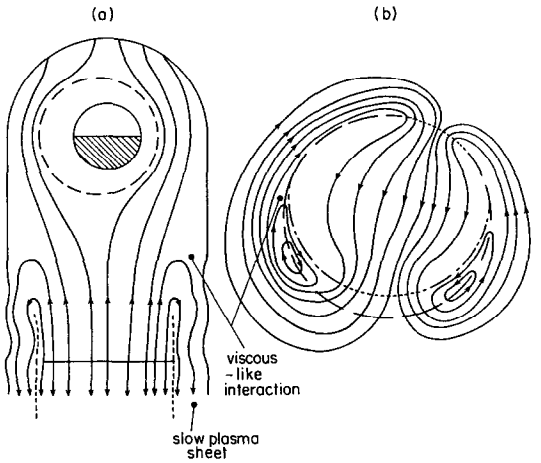

FIG. 9. SCHEMATIC OF VISCOUS INTERACTION EFFECTS ON CONVECTION SUGGESTED BY THE DATA PRESENTED BY RICHARDSON *et al.* (1988).
(a) The flow in the equatorial plane of the magnetotail and (b) a snapshot of the corresponding motion of the ionospheric feet of the field lines. The polar cap is considered as being in steady state.

(1988) provide some evidence for the interaction arising from Kelvin–Helmholtz waves, and they find no evidence of the additional plasma densities required by the hypothesis of penetration of solar-wind plasma or spatial diffusion from the sheath.

In part (b) of Fig. 9, a schematic of the expected flow streamlines in the ionosphere is given, corresponding to Fig. 9(a). Again, this is a snapshot at a particular time. The figure shows reconnection-driven cells, with plasma crossing the dayside merging gap and the nightside reconnection line (shown as dotted lines). The fact that the cap boundary was contracting in the period discussed in this paper indicates that there was an imbalance between the total merging rates at these two neutral lines, with more flux leaving the polar cap on the nightside than entering it on the dayside (see Lockwood and Freeman, 1988). However, a major duskward shift of the entire polar cap, for example under the influence of a strong swing to positive IMF B_y, may have the same effect, but seems unlikely. The schematic in Fig. 9(b), does not therefore correspond fully to the data, as the effects of the contraction of the cap have not been included (see Fig. 3 of Lockwood and Freeman, 1988). In Fig. 9, we consider the effects of the viscous-like interaction, without the cap contraction. The viscous-like interaction appears as a reversal in flow on closed field lines on the midnight side of dawn and dusk. Hence the boundary of open and closed field lines and the convection reversal no longer coincide. In this picture the number of closed field lines in the far magnetotail is continuously built up, i.e. the process feeds closed flux tubes from the nightside auroral zone into the antisunward-flowing polar cap, causing the separation of the convection reversal and the open field-line boundary to grow. At the particular time represented in Fig. 9(b) the convection reversal boundary is moving equatorward, and because ionospheric flow is incompressible, this gives a southward flow to the convection on closed field lines near midnight. Hence a viscous-driven cell is formed within the reconnection driven cell, as in the model by Reiff and Burch (1985) but which, from the Richardson *et al.* measurements, does not reach as far towards the dayside.

It must be emphasised that Fig. 9(b) is only a snapshot of the flow. It is known that the closed field lines cannot cycle around the viscous driven cells, because Richardson *et al.* observed the flows tailward of the neutral line to always be antisunward. Part (a) of Fig. 9 is also a snapshot, because it leads to an accumulation of closed field lines in the tail, off the bottom of the figure. At some time these must be pinched off and the near-Earth portion return earthward. The absence of sunward-moving closed field lines in the far tail, either in or out of the equatorial plane, suggests that the pinching-off does not occur continuously in the distant tail, beyond the neutral line, nor do the extended closed field lines move toward the centre of the tail and move earthward under magnetic tension. Rather, all anti-sunward closed field lines in the tail must be pinched off, possibly all at one time by the formation of a new neutral line which extends right across the magnetotail. In this case, the convection reversal will suddenly jump poleward, back to the open field line boundary, and the separation between the two will then grow again as the new neutral line retreats tailward and sunward-moving closed field lines are again exposed to the viscous interaction on the flanks of the tail. In this scenario, the ionospheric feet of some flux tubes would undergo the following motion. After emerging from the polar cap and being pulled sunward towards dawn or dusk in the usual manner, the tube would be slowed and turned antisunward by the viscous interaction, if it were close enough to the cap boundary. This would continue while the separation between the open field line boundary and the convection reversal grew, until the pinching-off occurred, when the flux tube is released from the viscous drag and moves sunward again. It is possible that a closed flux tube could undergo several of these cycles, before arriving at the dayside merging gap and re-entering the polar cap, causing a considerable increase in the residence time of some flux tubes in the region of auroral precipitation.

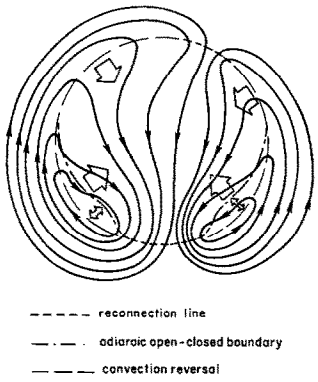

FIG. 10. SCHEMATIC OF A SNAPSHOT OF THE IONOSPHERIC FLOW WHEN VISCOUS INTERACTION AND POLAR CAP CONTRACTION ARE OCCURRING AT THE SAME TIME, AS IN THE EISCAT DATA PRESENTED IN THIS PAPER.

As mentioned above, the schematic shown in Fig. 9(b) does not fully describe the situation which is inferred from these EISCAT data. This is because in Fig. 9 there is viscous-like interaction on the flanks of the magnetotail, but the polar cap is in steady state (i.e. dayside and nightside reconnection rates are matched, see Lockwood and Freeman, 1988). In practice, the viscous merging may be most significant when the IMF is northward when the cap is likely to be contracting, as in the data presented here. Figure 10 combines the effect of the viscous-like interaction predicted in Fig. 9 with that of the cap contraction, as predicted by Lockwood and Freeman (1988), and therefore illustrates the type of convection pattern at the time of the EISCAT observations. In Fig. 10 the nightside reconnection potential exceeds that on the dayside (in fact, by a factor 11/4 in this illustration), the difference resulting in a contraction of the polar cap. This causes poleward convection at and near the poleward-moving adiaroic open-closed field-line boundaries.

There are two interesting features of the data presented, other than the poleward motion across the convection boundary, which may be explained by the above scenario. The first is the slowing of the flow at the boundary. This would correspond to the gradual slowing of the sunward moving closed field lines on the flanks of the tail by the viscous interaction, and their subsequent tailward acceleration to values typical of the slow plasma-sheet. However, it should be noted that a similar effect may be generated by the "shorting out" from the ionosphere of the viscous potential, caused by field-parallel potential differences between the ionosphere and the magnetosphere (Coley *et al.*, 1987). The second is the presence of wave-like oscillations in the boundary (with a period of about 40 min) and in the flow close to the boundary. Similar oscillations were observed close to the region of viscous-like interaction on the flanks of the tail by Richardson *et al.* (1988). In both cases these suggest that the viscous interaction may be due to Kelvin–Holmholtz waves on the boundary.

Lastly, it is interesting to compare the potential deduced in this paper with the values ascribed to viscous-like interaction in studies on the dependence of cross-cap potential on the interplanetary magnetic field and solar-wind velocity. Those studies show that when the IMF is northward there is still residual potential, even allowing for the time to lose open field lines which have remained connected through the far magnetotail to the IMF. The estimate of this residual potential of 35 kV by Reiff *et al.* (1981) was revised to about 15 kV by Wygant *et al.* (1983) by making allowance for the time constant of the decay of open flux tubes. In comparing the above values with the observations presented here, we must estimate the M.L.T. range over which the viscous interaction acts. The adiaroic cap boundary between the reconnection line on the nightside and the merging gap on the dayside covers about 6 h of M.L.T., in both the dawn and the dusk sector (Heelis *et al.*, 1982). If the potential were applied uniformly at 7 kV per 2 h and did not vary with time, this would be a total potential of 42 kV. This is similar to, although somewhat larger than, the values from the cross-cap potential studies, particularly those which allow for residual open field lines following a northward turning of the IMF, and larger than the maximum value of 30 kV reported by Mozer (1984, 1986). Richardson *et al.* (1988) conclude that the interaction only occurs on the flanks of the magnetotail, and not on the dayside, in which case the relevant segments of the cap boundary may be somewhat less than 6 h of M.L.T. long and 42 kV would then be an overestimate. In addition, Reiff and Luhmann (1986) suggest that the viscous potential on the dawn flank will be much greater than that on the dusk flank for the "garden-hose" orientation of the IMF, and this effect could reduce the total potential to nearer 20 kV, nearly all of which is applied on the dawn side. It is interesting to compare the peak value of 30 kV determined by Mozer (1984, 1986) with the average value of 3.1 kV (which is similar to the average of 2.5 kV derived by Coley *et al.*, 1987). Hence there is considerable variation in the viscous potential and the example presented here is at the large end of the range of reported values. Reiff and Luhmann (1986) have sorted the data of Mozer (1984) and found a strong dependence on the orientation of the sheath field, just outside the magnetopause. The average

potential is larger (7.5 kV) when this field is strongly northward, compared to an average of 1.5 kV at other times. The contraction of the polar cap at the time reported here argues for a northward IMF (see Lockwood and Freeman, 1988) in this case, however, simultaneous IMF data are not available (see Clauer *et al.*, 1988). The viscous potential is proportional to surface area of the flanks of the tail, it is possible that the neutral line in the tail was at great distances from the Earth during this period. Lastly, Sergeev and Kuznetsov (1981) have determined polar-cap potential from ground-based magnetometers and found a residual (viscous-like) term of $6(v/300)^2$, where v is the solar wind speed in km s^{-1}, giving 11 kV for a solar wind speed of 400 km s^{-1}. We infer that the segment of the cap boundary over which the viscous-like interaction acts is probably not much longer than the segment observed here (corresponding to 2 h of M.L.T.), giving a total potential which would then not be much larger than the 7 kV derived for the observed segment. In agreement with Richardson *et al.* (1988), we place most of this potential across the flanks of the tail (corresponding to the pre-dawn ionospheric polar cap boundary). It is also important to note that this is an average value over the 2 h during which the cap boundary was observed. Figure 7 indicates that there was considerable temporal variation within this period.

Acknowledgements—The authors are indebted to the EISCAT Director and his staff for operating the facility and supplying the data. EISCAT is an international facility supported by the research councils of Finland (SA), France (CNRS), the Federal Republic of Germany (MAG), Norway (NAVF), Sweden (NFR) and the U.K. (SERC). We are indebted to all EISCAT Associates for the contribution of Special Programme time for these observations. We also thank S. R. Crothers for the colour graphics. Support for Stanford University is provided by the National Science Foundation Grant ATM-8503105.

REFERENCES

Axford, W. I. and Hines, C. O. (1961) A unifying theory of high-latitude geophysical phenomena and geomagnetic storms. *Can. J. Phys.* **39**, 1433.

Brinton, H. C., Grebowsky, J. M. and Brace, L. H. (1978) The high-latitude winter *F*-region at 300 km: thermal plasma observations from AE-C. *J. geophys. Res.* **83**, 4767.

de la Beaujardiere, O., Evans, D. S., Kamide, Y. and Lepping, R. P. (1987) Response of the auroral oval precipitation and magnetospheric convection to changes in the interplanetary magnetic field. *Ann. Geophys.* **5A**, 519.

Clauer, C. R. and Banks, P. M. (1986) Relationship of the interplanetary electric field to the high latitude ionospheric electric field and currents: observations and model simulation. *J. geophys. Res.* **91**, 6959.

Clauer, C. R., Banks, P. M., Smith, A. Q., Jorgensen, T. S., Friis-Christensen, E., Vennerstrom, R., Wickwar, V. B., Kelley, J. D. and Doupnik, J. (1984) Observations of interplanetary magnetic field and of ionospheric plasma convection in the vicinity of the dayside polar cleft. *Geophys. Res. Lett.* **11**, 891.

Clauer, C. R., Kelley, J. D., Lockwood, M., Robinson, R. M., Ruohoniemi, J. M., de la Beaujardiere, O. and Hakkinen, L. (1988) June 1987 GISMOS experiment: preliminary report on high-time resolution, multi-radar measurements. *Adv. Space Res.* (in press).

Cole, K. D. (1974) Outline of a theory of solar-wind interaction with the magnetosphere. *Planet. Space Sci.* **22**, 1075.

Coley, W. R., Heelis, R. A., Hanson, W. B., Reiff, P. H., Sharber, J. R. and Winningham, J. D. (1987) Ionospheric convection signatures and magnetic field topology. *J. geophys. Res.* **92**, 12352.

Cowley, S. W. H. (1984) Solar wind control of magnetospheric convection, in *Achievements of the International Magnetospheric Study IMS*, pp. 483–494. ESA SP-217, ESTEC, Noordwijk, The Netherlands.

Cowley, S. W. H. (1986) The impact of recent observations on theoretical understanding of solar wind–magnetosphere interactions. *J. Geomagn. Geoelect.* **38**, 1223.

Crooker, N. U. (1977) The magnetospheric boundary layers: a geometrically explicit model. *J. geophys. Res.* **82**, 3629.

Doyle, M. A. and Burke, W. J. (1983) S3-2 measurements of polar-cap potential. *J. geophys. Res.* **88**, 9125.

Eastman, T. E. and Hones, E. W. Jr. (1979) Characteristics of the magnetospheric boundary layer as observed by *IMP6*. *J. geophys. Res.* **84**, 2019.

Etemadi, A., Cowley, S. W. H. and Lockwood, M. (1988a) The effect of rapid changes in ionospheric flow on velocity vectors deduced from radar beam-swinging experiments. *J. atmos. terr. Phys.* (submitted).

Etemadi, A., Cowley, S. W. H., Lockwood, M., Bromage, B. J. I., Willis, D. M. and Luhr, H. (1988b) The dependence of high-altitude dayside ionospheric flows on the North–South component of the IMF: a high time resolution correlation analysis using EISCAT "POLAR" and AMPTE UKS and IRM data. *Planet. Space Sci.* **36**, 471.

Eviatar, A. and Wolf, R. A. (1968) Transfer processes in the magnetopause. *J. geophys. Res.* **73**, 5561.

van Eyken, A. P., Rishbeth, H., Willis, D. M. and Cowley, S. W. H. (1984) Initial observations of plasma convection at invariant latitudes 70°–77°. *J. atmos. terr. Phys.* **46**, 635.

Gendrin, R. (1983) Magnetic turbulence and diffusion processes in the magnetospheric boundary layer. *Geophys. Res. Lett.* **10**, 769.

Geortz, C. K., Nielsen, E., Korth, A., Glassmeier, K. H., Haldoupis, C., Hoeg, P. and Hayward, D. (1985) Observation of a possible ground signature of flux transfer events. *J. geophys. Res.* **90**, 4069.

Heelis, R. A. and Hanson, W. B. (1980) High-latitude ion convection in the nightside *F*-region. *J. geophys. Res.* **85**, 1995.

Heelis, R. A., Hanson, W. B. and Burch, J. L. (1976) Ion convection reversals in the dayside cleft. *J. geophys. Res.* **81**, 3803.

Heelis, R. A., Lowell, J. K. and Spiro, R. W. (1982) A model of the high-latitude convection pattern. *J. geophys. Res.* **87**, 6339.

Heikkila, W. J. (1982) Inductive electric field at the magnetopause. *Geophys. Res. Lett.* **9**, 877.

Heikkila, W. J. (1986) Comment on electric field evidence

on the viscous interaction at the magnetopause, by F. S. Mozer. *Geophys. Res. Lett.* **13**, 233.

Heikkila, W. J. (1987) Neutral sheet crossings in the distant magnetotail, in *Magnetotail Physics* (Edited by Lui, A. T. Y.), p. 65. The Johns Hopkins University Press, Baltimore, Maryland.

Hill, T. W. (1983) Solar-wind magnetosphere coupling, in *Solar–Terrestrial Physics* (Edited by Carovillano, R. L. and Forbes, J. M.), p. 261. D. Reidel, Higham, Massachusetts.

Holzer, R. E., McPherron, R. L. and Hardy, D. A. (1986) A quantitative model of the magnetospheric flux transfer process. *J. geophys. Res.* **91**, 3287.

Jorgensen, T. S., Friis-Christensen, E., Wickwar, V. B., Kelly, J. D., Clauer, C. R. and Banks, P. M. (1984) On the reversal from "sunward" to "antisunward" plasma convection in the dayside high latitude ionosphere. *Geophys. Res. Lett.* **11**, 887.

Kelley, J. D. (1985) Incoherent scatter radar observations of the cusp, in *The Polar Cusp* (Edited by Holtet, J. A. and Egeland, A.). D. Reidel, Dordrecht.

Lemaire, J. (1987) Interpretation of the northward B_z (NBZ) Birkeland current system and polar-cap convection patterns in terms of the impulsive penetration model, in *Magnetotail Physics* (Edited by Lui, A. T. Y.), p. 83. The Johns Hopkins University Press, Baltimore, Maryland.

Lemaire, J. and Roth, S. (1978) Penetration of solar wind plasma elements into the magnetosphere. *J. atmos. terr. Phys.* **40**, 331.

Lockwood, M. and Freeman, M. P. (1988) Recent ionospheric observations relating to solar wind–magnetosphere coupling. *Phil. Trans. R. Soc.* (*London*) **A** (in press).

Lockwood, M. and Fuller-Rowell, T. J. (1987a) The modelled occurrence of non-thermal plasma in the ionospheric *F*-region and possible consequences for ion outflows into the magnetosphere. *Geophys. Res. Lett.* **14**, 371.

Lockwood, M. and Fuller-Rowell, T. J. (1987b) Correction to "The modelled occurrence of non-thermal plasma in the ionospheric *F*-region and possible consequences for ion outflows into the magnetosphere". *Geophys. Res. Lett.* **14**, 581.

Lockwood, M., Bromage, B. J. I., Horne, R. B., St-Maurice, J.-P., Willis, D. M. and Cowley, S. W. H. (1987) Non-Maxwellian ion velocity distributions observed using EISCAT. *Geophys. Res. Lett.* **14**, 111.

Lockwood, M., van Eyken, A. P., Bromage, B. J. I., Waite, J. H., Jr., Moore, T. E. and Doupnik, J. R. (1986) Low-energy ion outflows from the ionosphere during a major cap expansion—evidence for equatorward motion of inverted-V structures. *Adv. Space Res.* **6**, 93.

Lockwood, M., Smith, M. F., Farrugia, C. J. and Siscoe, G. L. (1988a) Ionospheric ion upwelling in the wake of Flux Transfer Events at the dayside magnetopause. *J. geophys. Res.* **93**, 5641.

Lockwood, M., Suvanto, K., St-Maurice, J.-P., Kikuchi, K., Bromage, B. J. I., Willis, D. M., Crothers, S. R., Todd, H. and Cowley, S. W. H. (1988b) Scattered power from non-thermal, *F*-region plasma observed by EISCAT—evidence for coherent echoes? *J. atmos. terr. Phys.* **50**, 467.

Lockwood, M., Suvanto, K., Cowley, S. W. H., Horne, R. B., Bromage, B. J. I., Willis, D. M. and St-Maurice, J.-P. (1988c) Incoherent scatter observations of non-Maxwellian ion velocity distribution in the auroral *F*-region of the ionosphere. *J. geophys. Res.* (submitted).

Meng, C.-I., Holzworth, R. H. and Akasofu, S.-I. (1977) Auroral circle-delineating the boundary of the quiet auroral belt. *J. geophys. Res.* **82**, 164.

Mozer, F. S. (1984) Electric field evidence for viscous interaction at the magnetopause. *Geophys. Res. Lett.* **11**, 981.

Mozer, F. S. (1986) Reply to comment on electric field evidence for viscous interaction at the magnetopause. *Geophys. Res. Lett.* **13**, 235.

Olson, W. P. and Pfitzer, K. A. (1985) Magnetospheric response to the gradient drift entry of sold wind plasma. *J. geophys. Res.* **90**, 10823.

Pu, Z.-U. and Kivelson, M. G. (1983) Kelvin–Helmholtz instability at the magnetopause: solution for compressible plasmas. *J. geophys. Res.* **88**, 841.

Raman, R. S. V., St. Maurice, J.-P. and Ong, R. S. B. (1981) Incoherent scattering of radar waves in the auroral ionosphere. *J. geophys. Res.* **86**, 4751.

Reiff, P. H. and Burch, J. L. (1985) IMF B_y-dependent plasma flow and Birkeland current in the dayside magnetosphere. 2—A global model for northward and southward IMF. *J. geophys. Res.* **90**, 1595.

Reiff, P. H. and Luhmann, J. G. (1986) Solar-wind control of the polar-cap voltage, in *Solar Wind-Magnetosphere Coupling* (Edited by Kamide, Y. and Slavin, J. A.), p. 452. Terra Scientifica, Tokyo, 1986.

Reiff, P. H., Spiro, R. W. and Hill, T. W. (1981) Dependence of polar-cap potential drop on interplanetary parameters. *J. geophys. Res.* **86**, 7639.

Reiff, P. H., Spiro, R. W., Wolf, R. A., Kamide, Y. and King, J. H. (1985) Comparison of polar-cap potential drops estimated from solar wind and ground magnetometer data. *J. geophys. Res.* **90**, 1318.

Richardson, I. G., Owen, C. J., Cowley, S. W. H., Galvin, A. B., Sanderson, T. R., Scholer, M., Slavin, J. A. and Zwickl, R. D. (1988) *ISEE*-3 observations during the CDAW-8 intervals: case studies of the distant geomagnetic tail covering a wide range of geomagnetic activity. *J. geophys. Res.* (submitted).

Russell, C. T. and Elphic, R. C. (1978) Initial ISEE magnetometer results: magnetopause observations. *Space Sci. Rev.* **22**, 681.

Sanders, G. D., Maker, L. J. and Freemand, J. W. (1980) Observation of the plasma boundary layer at lunar distances: direct injection of plasma into the plasma sheet. *J. geophys. Res.* **85**, 4607.

Schunk, R. W., Raitt, W. J. and Banks, P. M. (1975) Effect of electric fields on the daytime high-latitude *E* and *F* regions. *J. geophys. Res.* **80**, 3121.

Sergeev, V. A. and Kuznetsov, B. M. (1981) Quantitative dependence of the polar cap electric field on the IMF B_z component and solar wind velocity. *Planet. Space Sci.* **29**, 205.

Siscoe, G. L. and Huang, T. S. (1985) Polar-cap inflation and deflation. *J. geophys. Res.* **90**, 543.

Slavin, J. A., Smith, E. J., Sibeck, D. G., Baker, D. N., Zwickl, R. D. and Akasofu, S.-I. (1985) An *ISEE*-3 study of average and substorm conditions in the distant magnetotail. *J. geophys. Res.* **90**, 10875.

Southwood, D. J. (1985) Theoretical aspects of ionosphere-magnetosphere-solar wind coupling. *Adv. Space Res.* **5**, 7.

Southwood, D. J. (1987) The ionospheric signature of flux transfer events. *J. geophys. Res.* **92**, 3207.

Southwood, D. J., Farrugia, C. J. and Saunders, M. A. (1988) What are flux transfer events? *Planet Space Sci.* **36**, 503.

Suvanto, K. (1988) Incoherent scattering of radar waves

from non-thermal plasma. *Radio Sci.* (in press).

Suvanto, K., Lockwood, M., Winser, K. J., Farmer, A. D. and Bromage, B. J. I. (1988) Analysis of incoherent scatter radar data from non-thermal F-region plasma. *J. atmos. terr. Phys.* (submitted).

Todd, H., Bromage, B. J. I., Cowley, S. W. H., Lockwood, M., van Eyken, A. P. and Willis, D. M. (1986) EISCAT observations of bursts of rapid flow in the high latitude dayside ionosphere. *Geophys. Res. Lett.* **13**, 909.

Todd, H., Cowley, S. W. H., Etemadi, A., Bromage, B. J. I., Lockwood, M., Willis, D. M. and Luhr, H. (1988) Flow in the high-latitude ionosphere: measurements at 15 s resolution made using the EISCAT "POLAR" experiment. *J. atmos. terr. Phys.* **50**, 423.

Tsurutani, B. T. and Thorne, R. M. (1982) Diffusion processes in the magnetospheric boundary layer. *Geophys. Res. Lett.* **9**, 1247.

Willis, D. M., Lockwood, M., Cowley, S. W. H., van Eyken, A. P., Bromage, B. J. I., Rishbeth, H., Smith, P. R. and Crothers, S. R. (1986) A survey of simultaneous observations of the high-latitude ionosphere and Interplanetary Magnetic Field with EISCAT and AMPTE-UKS. *J. atmos. terr. Phys.* **48**, 987.

Wygant, J. R., Torbert, R. B. and Mozer, F. S. (1983) Comparison of S3-3 polar cap potential drops with the interplanetary magnetic field and models of magnetopause reconnection. *J. geophys. Res.* **88**, 5727.